European Journal of Medicinal Chemistry 72 (2014) 146–159

Contents lists available at ScienceDirect

European Journal of Medicinal Chemistry

journal homepage: http://www.elsevier.com/locate/ejmech

Original article

A development of chimeric VEGFR2 TK inhibitor based on two ligand conformers from PDB: 1Y6A complex – Medicinal chemistry consequences of a TKs analysis

Lucia Lintnerová [a], Melissa García-Caballero [b,1], Fridrich Gregáň [c], Milan Melicherčík [c], Ana R. Quesada [b,1], Juraj Dobiaš [a], Ján Lác [d], Marta Sališová [a], Andrej Boháč [a,d,*,2]

[a] Comenius University, Faculty of Natural Sciences, Department of Organic Chemistry, Mlynská dolina, 842 15 Bratislava, Slovakia
[b] Departamento de Biología Molecular y Bioquímica, Facultad de Ciencias, Universidad de Málaga, Campus de Teatinos, 29071 Málaga, Spain
[c] Matej Bel University, Faculty of Natural Sciences, Department of Chemistry Tajovského 40, 974 01 Banská Bystrica, Slovakia
[d] Biomagi, Inc., Mamateyova 26, 851 04 Bratislava, Slovakia

ARTICLE INFO

Article history:
Received 30 May 2013
Received in revised form
3 November 2013
Accepted 20 November 2013
Available online 1 December 2013

Keywords:
Angiogenesis sorafenib Nexavar sunitinib Sutent oxazole
Properties of VEGFR-2 tyrosine kinase variants
Flexible tyrosine kinase activation loop
Type I inhibitor DFG-out A-loop/ligand collision
Medicinal chemistry consequences

ABSTRACT

VEGFR2 is an important mediator of angiogenesis and influences fate of some cancer stem cells. Here we analysed all 34 structures of VEGFR2 TK available from PDB database. From them a complex PDB: 1Y6A has an exceptional **AAZ** ligand bound to TK in form of two conformers (*U*- and *S*-shaped). This observation inspired us to develop three chimeric bispyridyl VEGFR2 inhibitors by combining structural features of both **AAZ** conformers and/or their relative ligand **AAX** (PDB: 1Y6B).

Our most interesting inhibitor **22SYM** has an enzymatic VEGFR2 TK activity (IC_{50}: 15.1 nM) comparable or better to the active compounds from clinical drugs Nexavar and Sutent. **22SYM** inhibits growth, migration and tube formation of endothelial cells (EC) and selectively induces EC apoptosis. **22SYM** also inhibits *in vivo* angiogenesis in Zebrafish embryo assay.

Additionally to the above results, we proved here that tyrosine kinases in an inactive form possessing Type I inhibitors can adopt both a closed or an opened conformation of kinase A-loop independently on their DFG-out arrangement. We proposed here that an activity of certain Type I inhibitors (e.g. **22SYM**-like) in complex with DFG-out TK can be negatively influenced by collisions with a dynamically moving TK A-loop.

1. Introduction

VEGFR2 is considered a key receptor for VEGF signal transduction by angiogenesis [1,2]. Inhibition of VEGFR2 receptor was recently predicted to influence in part the fate of the human glioma cancer stem cells [3].

2-Anilino-5-aryloxazoles represent a class of potent VEGFR2 kinase inhibitors possessing good enzymatic and cellular activities. Among them, the compound **AAZ** in form of its bis-mesylate salt showed good solubility, pharmacokinetic profiles and moderate efficacy in preliminary *in vivo* xenograft studies. **AAZ** inhibitor has shown good enzymatic (IC_{50} = 22 nM, VEGFR2) and cellular activity (IC_{50} = 370 nM, HUVEC/VEGF) [4]. X-ray structures of relative 2-anilino-5-aryloxazole ligands **AAZ** and **AAX** in complex with VEGFR2 TK are available in Protein Data Bank (PDB: 1Y6A, 1Y6B, resp.) [5]. The crystallography study confirmed binding mode of both ligands in ATP binding site of VEGFR2 tyrosine kinase.

The 3D structure of tyrosine kinases can be found in an active or inactive conformation based on 3D arrangement of a conserved DFG fragment located at their activation loop (A-loop). The A-loop can be generally defined as beginning with the residues DFG (Asp-Phe-Gly) and ending at the conserved APE (Ala-Pro-Glu) sequence. Particularly the A-loop in VEGFR2 tyrosine kinase (PDB: 1Y6A) consists from 30 amino acid residues: Phe1044–Glu1073 [5]. Active (DFG-in) kinases have a Phe residue from DFG fragment positioned under their αC-helix and the catalytic aspartic acid points into the ATP binding pocket (Fig. 8). When the DFG flips in an inactive DFG-out conformation, the Phe side chain moves away and occupies the

* Corresponding author. Comenius University, Faculty of Natural Sciences, Department of Organic Chemistry, Mlynská dolina, 842 15 Bratislava, Slovakia. Tel.: +421 260296409; fax: +421 260296337.
E-mail addresses: fridrich.gregan@umb.sk (F. Gregáň), milan.melichercik@umb.sk (M. Melicherčík), quesada@uma.es (A.R. Quesada), andrej.bohac@fns.uniba.sk (A. Boháč).
[1] Tel.: +34 (9)52137128; fax: +34 (9)52132000.
[2] Tel.: +421 902522144.

0223-5234/$ – see front matter © 2013 Elsevier Masson SAS. All rights reserved.
http://dx.doi.org/10.1016/j.ejmech.2013.11.023

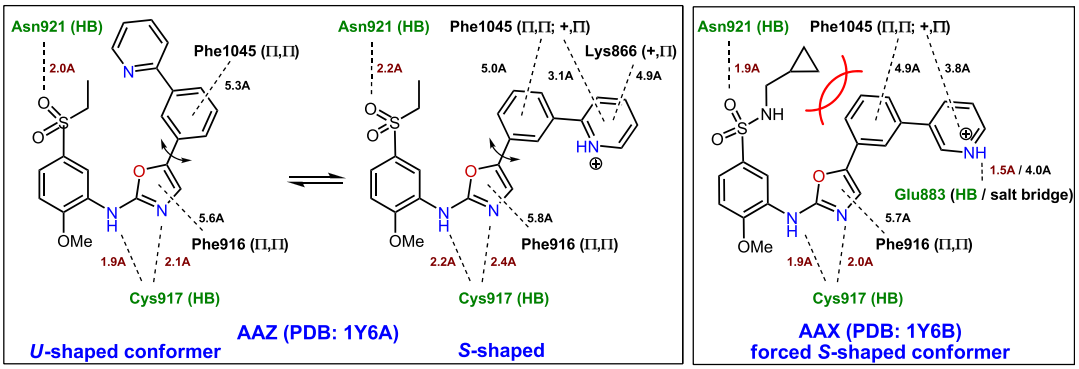

Fig. 1. The maps of intermolecular interactions of **AAZ** and **AAX** ligands within appropriate VEGFR2 TK protein variants (hydrogen bonds, stacked (Π, Π), induced dipole (+, Π) and salt bridge linkages are depicted, no liphophilic interactions are shown). In the left: Two active conformers (*U*- and *S*-shaped) of **AAZ** ligand (PDB: 1Y6A). In the right: **AAX** ligand (PDB: 1Y6B) possesses only *S*-shaped active conformation due to the bulky *N*-cyclopropylmethyl substituent used in **AAX** structure as conformation blocker.

oppositely positioned ATP kinase pocket (Fig. 9 or 10). The conformational flexibility of the DFG motif allows adopting several "in" or "out"-like conformations. The active and inactive kinase variants are sometimes less exactly, as we have shown here, characterized in the literature by an opened or a closed A-loop conformation, resp. independently on 3D arrangement of their DFG fragment. The equilibrium between DFG-in and DFG-out forms can be controlled by the nature of inhibitor present in a complex with protein. Type I inhibitors are mimicking the ATP adenine ring in its interactions with "hinge" amino acid residues of a tyrosine kinase (in PDB: 1Y6A VEGFR2 variant numbering: HB-bonds with e.g. Glu915 and Cys917). Type I inhibitors are normally targeting the ATP binding site of a tyrosine kinase in its active (DFG-in) form. In some cases Type I inhibitors can also bind to an inactive (DFG-out) kinase (e.g. Table 3, PDBs: 1Y6A, 1Y6B, 3CJF, 3C7Q, 3VID and 4AGD). Type II inhibitors bind exclusively an inactive DFG-out kinase form and stabilize its conformation. They bind the same area occupied by the Type I compounds but also extends to the additional hydrophobic site available in the DFG-out kinase (e.g. Table 3, PDBs: 1YWN, 2P2I, 2OH4 etc.). Type III inhibitors bind an allosteric back pocket of Type II inhibitors (positioned under αC-helix) without occupying ATP binding place (e.g. Table 3, PDB: 3VHK). Novel Type I1/2 inhibitors are present exclusively in an active DFG-in kinases and bind to the ATP binding site like Type I compounds and then extend into the back cavity of the ATP site to give specific interactions with those residues that are partially involved in the Type II pharmacophore present in DFG-out kinases (e.g. Table 3, PDB: 3B8R) [6].

Currently the PDB database contains 1 human intracellular VEGFR2 TK (tyrosine kinase) protein and 33 crystal structures of intracellular VEGFR2 tyrosine kinase/ligand complexes [5]. Among all 33 VEGFR2 TK complexes only PDB: 1Y6A shows population of two structures of **AAZ** ligand in co-crystals with VEGFR2 TK protein. Presence of the two different **AAZ** conformers within the kinase structure indicates that the active structures of **AAZ** could be represented by two distinct rotamers. Both conformers of **AAZ** differ mainly in an orientation of the terminal pyridyl substituent (*U*- or *S*-shaped) (Fig. 1).

To develop inhibitor mimicking both conformers in one structure (e.g. **22SYM**) with ability to occupy both possible binding poses in VEGFR2 TK protein attracted our attention.

2. Results and discussion

2.1. Structure analysis

In order to understand the relation between ligands and proteins, interaction analyses of conformations of **AAZ** and **AAX** ligand were performed in appropriate VEGFR2 tyrosine kinase variants from PDB complexes (1Y6A and 1Y6B, resp.) (Fig. 1).

U-shaped conformation of AA**Z** ligand has a packed form and its pyridyl substituent is oriented towards the entrance, a solvent accessible part, of the ATP binding site of VEGFR2 TK. The *U*-shaped **AAZ** conformer has three hydrogen bonds and two stabilizing stacked interactions with two Phe amino acid residues originating from the VEGFR2 kinase. Pyridyl substituent from the *U*-shaped **AAZ** conformer is oriented in direction of possible A-loop position (PDB: 1Y6B, Asp1044–Glu1073) [7]. In both PDB complexes 1Y6A and 1Y6B their A-loops are mostly disordered due to their flexibility. *S*-shaped conformer of **AAZ** ligand is more buried into the VEGFR2 protein. This conformer has three hydrogen bonds that seem to be less strong, while phenylpyridyl substituent possesses more possible intermolecular interactions compare to its *U*-shaped conformer (Fig. 1).

Two conformers of **AAZ** ligand (*U*- and *S*-shaped) occupying two partially different poses in the VEGFR2 TK protein (PDB: 1Y6A). A superimposition of both conformers showed their relative positions in VEGFR2. While their arylaminooxazole parts are well overlapped (low parts of the superimposed structures on Fig. 2), their phenyl rings (each bearing pyridyl substituent) are twisted off the coplanarity at about 24° (Fig. 2, the right part).

2.2. Design of chimeric compounds

We designed bispyridyl ligands with an aim to occupy both binding poses of two conformers observed in VEGFR2 TK complex PDB: 1Y6A. For this purpose we combined pyrid-2-yl and pyrid-3-yl substituents undertaken from the structures of relative ligands **AAZ** and **AAX** (PDB: 1Y6A and 1Y6B, resp.). We decided to prepare and screen new chimeric bispyridyl compounds **22SYM**, **23ASYM** and **33SYM**. Before the synthesis, we estimated drug-like properties for all structures by freely available prediction toolkit Molinspiration [8]. We determined that all three isomeric compounds seemed to be appropriate with exception of their molecular weight (FW: 512.59) that was slightly higher as recommended. Bispyridyl compounds **22SYM**, **23ASYM**, **33SYM** possess miLogP in scope of 4.72–4.87. The second introduced pyridyl ring slightly increases lipophilicity of chimeric molecules compare with monopyridyl compound **AAZ** (miLog P = 4.12). The presence of the second pyridyl group can help to improve the solubility in water (e.g. in case of their tris-mezylate salts). All designed compounds have other predicted parameters in accordance within recommended drug-like values: TPSA (polar surface area) = 107.2 Å^2, nOH = 8 (number of hydrogen bond accepting atoms), nOHNH = 1 (number of hydrogen bond donating hydrogens) and NRB = 8 (number of

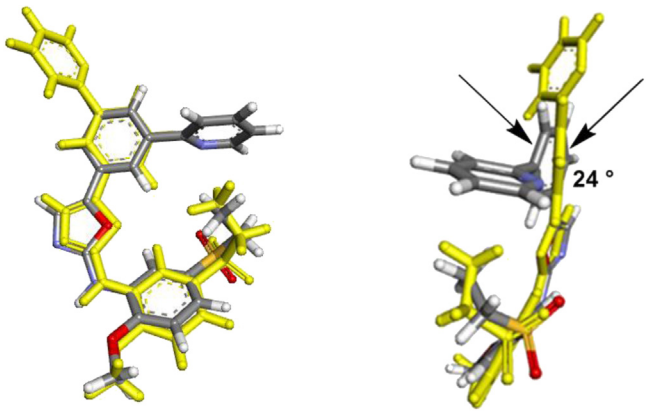

Fig. 2. Two superimposed conformers of **AAZ** ligand (PDB: 1Y6A) in front and side view, resp. *U*-shaped conformer is coloured by atoms and *S*-shaped rotamer is coloured in yellow. The phenyl rings bearing pyridyl substituent of both conformers are deviated from coplanarity at about 24° (visible on the structures in the right).

rotatable bonds, responsible for the amount of possible conformers) [8].

The structures of all chimeric compounds **22SYM**, **23ASYM**, **33SYM** together with their synthetic intermediate **8** and ligands **AAZ** and **AAX** were docked into both VEGFR-2 protein variants (PDB: 1Y6A, 1Y6B). A final docking experiment was carried out in VEGFR2 receptor variant from the complex PDB: 1Y6B, because this one showed better quality in a calibration docking compare with the protein variant originating from the complex PDB: 1Y6A (Fig. 3).

The docking experiment was performed with the VEGFR2 protein variant from a complex (PDB: 1Y6B) possessing **AAZ** ligand that is structurally close to the designed bispyridyl compounds **22SYM**, **23ASYM** and **33SYM**. Therefore, we did not expect high impact of a ligand driven induced fit on the active side of the kinase that can be responsible for prediction inaccuracy [9–11]. The values of score resulted from the docking in VEGFR2 variant (PDB: 1Y6B) were markedly better for **22SYM**, **23ASYM** and **33SYM** (−60.1 to −58.4 kcal/mol, Fig. 3) than the obtained values for a native inhibitor **AAX** (−50.3 kcal/mol) and its relative compound **AAZ** (−52.9 kcal/mol).

Because the possibility that **22SYM**, **23ASYM** and **33SYM** will occupy both VEGFR2 **AAZ** conformational binding poses and their high score obtained from the docking experiment we expected better IC_{50} activities for our bispyridyl compounds compare to the activity of **AAZ** ligand possessing only one pyridyl group in its structure.

2.3. Synthesis

Synthesis of **22SYM** and its analogues **23ASYM**, **33SYM** was performed from commercially available compounds (Scheme 1). Because 5-(ethylsulfonyl)-2-methoxyaniline (**5a**) used for the preparation of the key oxazolaryldibromo intermediate **6** was not sufficiently available, recently we developed its synthesis [12].

Commercially available *p*-aminoacetophenone (**1**) was transformed to dibromoaniline **2** by bromine in acetic acid in 74% yield. Subsequently amino group from aniline **2** was removed by diazotation in the presence of Cu powder in refluxing EtOH within 12 h to give 3,5-dibrominateted acetophenone **3** in 60% yield. An aliphatic chain bromination of acetophenone **3** was performed by bromine in Et_2O at rt in 68% yield. Bromine on aliphatic chain of **4** was substituted by sodium azide at 0 °C in MeOH within 2.5 h in 81% yield. Azide **5** was transformed by 4-(ethylsulfonyl)-2-isocyanato-1-methoxybenzene (**5b**) in the presence of PPh_3 in DCM at rt within 1 h to oxazole **6** in 19% yield. By this reaction a urea compound **7** was obtained as a side product in 26% yield. Urea compound **7** was stable and not possible in our hands to transform to desired compound **6**. 4-(Ethylsulfonyl)-2-isocyanato-1-methoxybenzene (**5b**) requested for synthesis of **6** was prepared

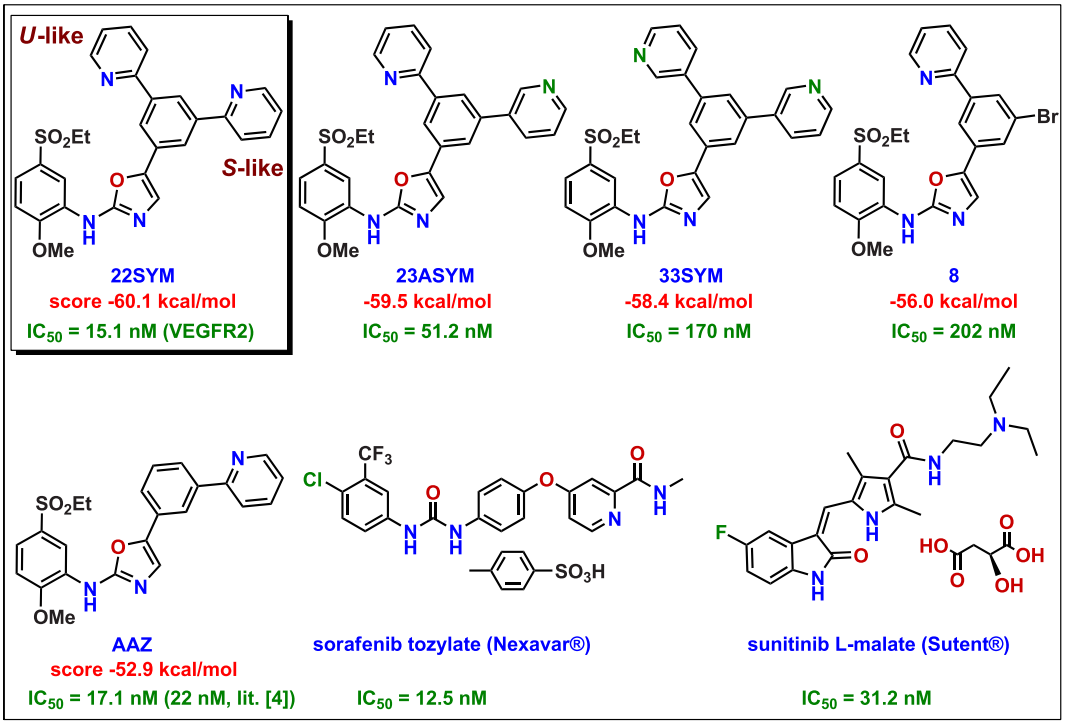

Fig. 3. The structures, docking scores and determined enzymatic VEGFR2 activities for chimeric compounds **22SYM**, **23ASYM**, **33SYM** and **8** in comparison with **AAZ** standard and active components of clinical drugs sorafenib tosylate (Nexavar®, Bayer, FDA approved in Dec. 2005) and sunitinib L-malate (Sutent®, Pfizer, FDA approved in Jan. 2006).

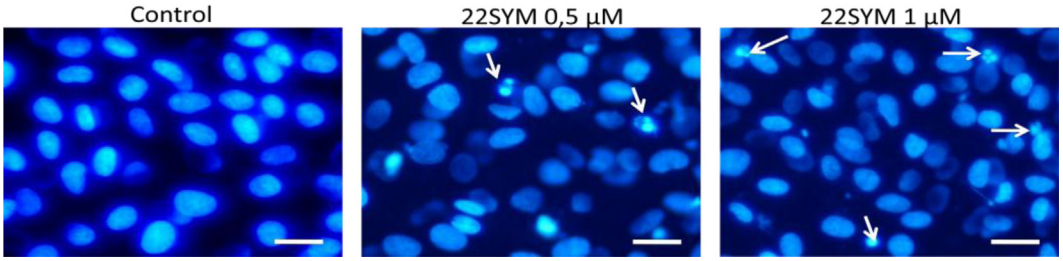

Fig. 4. Effect of **22SYM** on endothelial cell morphology (Hoechst staining) (bar = 50 μm).

in 98% yield by reaction of 5-(ethylsulfonyl)-2-methoxyaniline (**5a**) with 20% phosgene solution in toluene (first the starting aniline **5a** was added in EA solution into 0 °C cold phosgene solution (3.0 mol eq, 20% phosgene in toluene), then the reaction mixture was refluxed within 3 h). Final products **22SYM** and **33SYM** were synthesized from aminooxazole **6** each in one step by either Stille reaction with Bu_3Snpy-2-yl (56%) or Suzuki reaction with $(HO)_2Bpy$-3-yl (58%), respectively. Both coupling reactions were carried out in the presence of $(PPh_3)_4Pd$. Compound **23ASYM** was prepared in two independent Stille coupling reaction steps. First aminooxazole **6** was transformed to compound **8** with Bu_3Snpy-2-yl (52%) and subsequently **8** converted to compound **23ASYM** by reaction of **8** with Bu_3Snpy-3-yl in 62% yield.

2.4. Biological results

2.4.1. In vitro VEGFR2 kinase assay

A radiometric protein kinase assay (^{33}PanQinase® Activity Assay) was used for measuring the kinase activity of the VEGFR2 protein. The IC_{50} profile of four compounds **22SYM**, **23ASYM**, **33SYM** and **8** was determined by testing at 10 concentrations (1×10^{-4} M to 3×10^{-9} M) for each compound. All compounds bind selectively to VEGFR2 tyrosine kinase by concentration dependent manner. The measurements have been performed by ProQinase Company [13]. IC_{50} values were found in the range from 15.1×10^{-9} M to 202×10^{-9} M (Fig. 3).

2.4.2. ***22SYM*** *selectively inhibits endothelial cells growth*

Angiogenesis involves local proliferation of endothelial cells. We investigated the ability of **22SYM** to inhibit the growth of endothelial and tumour cells. IC_{50} values of this antiproliferative effect are shown in Table 1. **22SYM** inhibits endothelial cell growth at submicromolar concentrations (IC_{50} = 370 nM, BAEC/VEGF). Comparison of the results with those obtained with tumour cells suggests that this inhibitory effect is exerted preferentially on endothelial cells, since the values of IC_{50} obtained for the tumour cell lines were mostly at least one order of magnitude higher than that for BAEC.

2.4.3. ***22SYM*** *induces endothelial cells apoptosis*

The induction of endothelial apoptosis is a common mechanism exhibited by a number of angiogenesis inhibitors. As a first approach to determine whether **22SYM** could induce apoptosis in endothelial cells, nuclear morphology was investigated in BAE cells after 14 h treatment with different concentrations of this compound. Fig. 4 shows that **22SYM** concentrations of 0.5 μM or higher, induced chromatin condensation in endothelial cells that is a sign of apoptosis.

2.4.4. ***22SYM*** *inhibits the migratory capability of endothelial cells*

Angiogenesis involves the acquisition by endothelial cells of the capability to migrate through extracellular matrix, degrade the basement membrane and, in general, to remodel the extracellular matrix. As shown in Figs. 5, 1 μM **22SYM** produced a significant inhibition of the migratory capability of BAEC.

2.4.5. ***22SYM*** *inhibits the endothelial cells capillary tube formation*

The final event during angiogenesis is the organization of endothelial cells in a three-dimensional network of tubes. *In vitro*, endothelial cells plated on Matrigel align themselves forming cords, already evident a few hours after plating. Fig. 6 shows that 1 μM **22SYM** was able to completely inhibit the BAE cell alignment and cord formation.

2.4.6. ***22SYM*** *inhibits in vivo angiogenesis in the Zebrafish embryo assay*

To evaluate the *in vivo* antiangiogenic activity of **22SYM**, different concentrations of this compound were incubated with embryos from a transgenic Zebrafish line with GFP expression in the endothelium. As shown in Table 2, the systemic exposure of **22SYM** exerted a dose–response inhibitory effect on the developmental angiogenesis in Zebrafish. During development of the Zebrafish, intersegmental vessels sprout and grow upward from the aorta, and then the tips join by anastomosis to form a dorsal vein. Our results show that 10 μM **22SYM** inhibited the Zebrafish intersegmental blood vessel growth and angiogenesis, although the

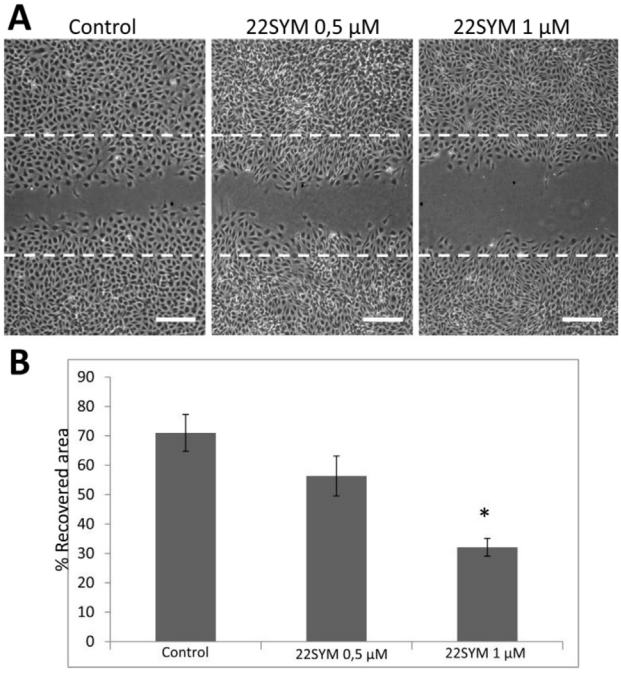

Fig. 5. 22SYM inhibits the migratory capabilities of endothelial cells (A) Confluent BAEC monolayers were wounded and fresh culture medium was added either in the absence or presence of the indicated concentrations of **22SYM**. Photographs were taken at the beginning of the assay and after 7 h of incubation. Broken lines indicate the wound edges (bar = 200 μm) (B) The regrowth of BAEC into the cell-free area was measured after 7 h and percentages of recovered area are expressed as mean ± SD, $^*P < 0.001$ versus control ($n = 3$).

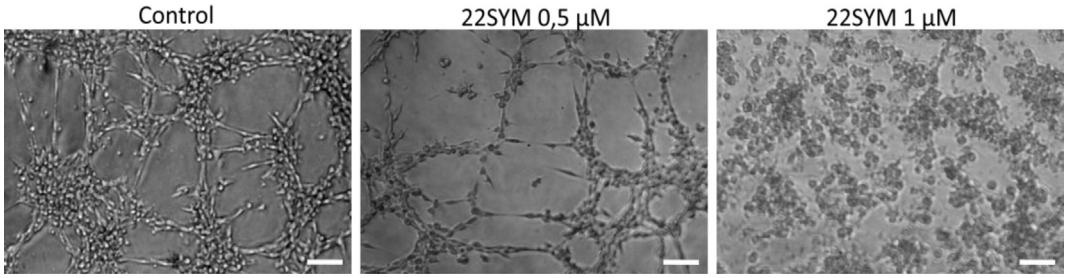

Fig. 6. Endothelial cell tube formation. BAEC seeded on Matrigel formed tubes (left panel). **22SYM** inhibited endothelial cell tubulogenesis *in vitro* in a dose-dependent manner at non-toxic doses (bar = 100 μm).

embryos remained viable during the 24-h period of the study and overall morphology was similar to control embryos, indicating that development was unaffected and also indicating a low toxicity of this compound (Fig. 7). Data are given as percentage of embryos with inhibited angiogenesis per total number of treated Zebrafish embryos.

2.5. Predicted & obtained VEGFR2 activity

After the VEGFR enzymatic activity was performed [13], we found that our best inhibitor **22SYM** (IC_{50}: 15.1 nM) was only slightly more active than the current inhibitor **AAZ** (IC_{50}: 17.1 nM) (Fig. 3). We proposed two factors that can be responsible for the difference between expected and obtained VEGFR2 activity for our chimeric compound **22SYM**:

a/the docking experiment was performed on the VEGFR2 protein variant taken from the PDB: 1Y6B complex. Both complexes 1Y6A and 1Y6B contain similar protein kinase variants that do not have sufficiently rigid activation loop (A-loop) and therefore this part of the protein is not visible in their X-ray structures. The docking experiment was performed without information about the position of this loop. A-loop in an unfavourable case, as we show later, can get to a close proximity of **22SYM** ligand and cause a collision between parts of the A-loop and **22SYM** inhibitor (e.g. Fig. 10). Despite high predicted docking score for compound **22SYM** (Fig. 3), flexible, dynamically moving tyrosine kinase A-loop hitting **22SYM** ligand in a kinase complex can markedly diminish its averaged inhibitory activity determined in a biological assay.

b/**22SYM** represents a chimeric compound derived from the two conformers of **AAZ** (PDB: 1Y6A) ligand. The superimposed conformers of **AAZ** differ markedly in the position of their pyridyl substituent. They differ also in a position of phenyl ring bearing the pyridyl substituent. We determined that phenyl rings originating from two conformers are deviated from their coplanarity at about 24° (Fig. 2). The bispyridyl **22SYM** ligand possesses *U*-like and *S*-like pyridyl substituents (Fig. 3). Its in Silico predicted position has the phenyl ring bearing both pyridyl substituents for **22SYM** in almost identical position (not shown) with experimental coordinates of the phenyl ring bearing pyrid-2-yl substituent in the *S*-shaped conformer of **AAZ** ligand (Fig. 2). Therefore, **22SYM** ligand should has its *U*-like pyridyl group more buried into a VEGFR2 kinase compare to the opposite case when higher pose similarity to the *U*-shaped conformer of **AAZ** ligand would be preferred by computer prediction (Fig. 2). Therefore, we can expect that the *U*-shaped pyridyl group in **22SYM** is oriented more closely to a possible position of a flexible A-loop of VEGFR2 kinase and collisions between A-loop and **22SYM** are more likely to expect.

2.6. Analysis of 34 VEGFR2 tyrosine kinase variants

We superimposed and analysed all 34 PDB available VEGFR2 TK structures in order to explain possible collisions of a flexible A-loop with **22SYM** ligand. **22SYM** is a Type I inhibitor that can be possibly adopted by both an active and an inactive kinase forms [5,6]. Within our analysis, we observed that VEGFR2 protein variants are in a complex with different types of inhibitors (or fragments): Type I (8 complexes), Type I 1/2 (1), Type II (23) and Type III (1) [6,14]. In the kinase active form, the DFG motif adopts the DFG-in conformation in which the catalytic aspartic acid points into the ATP binding pocket and the phenylalanine points away from the ATP.

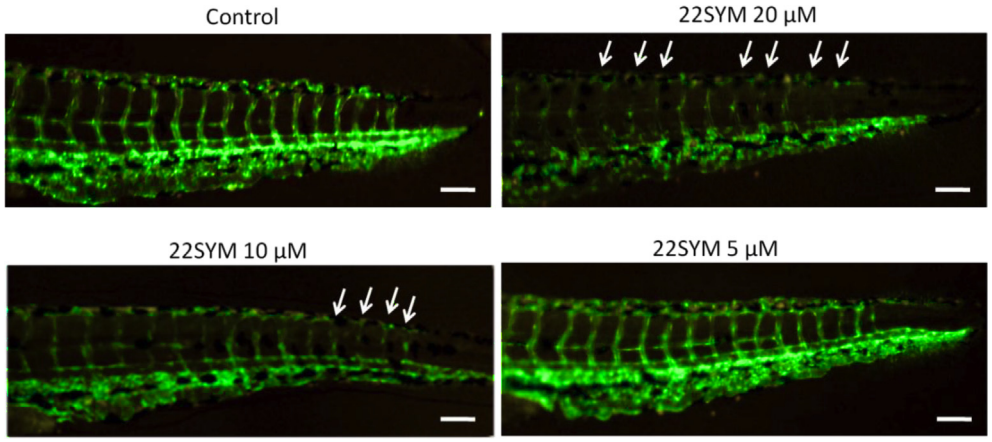

Fig. 7. Inhibitions of the Zebrafish embryo neovascularisation by **22SYM**. Bars represent 50 μm.

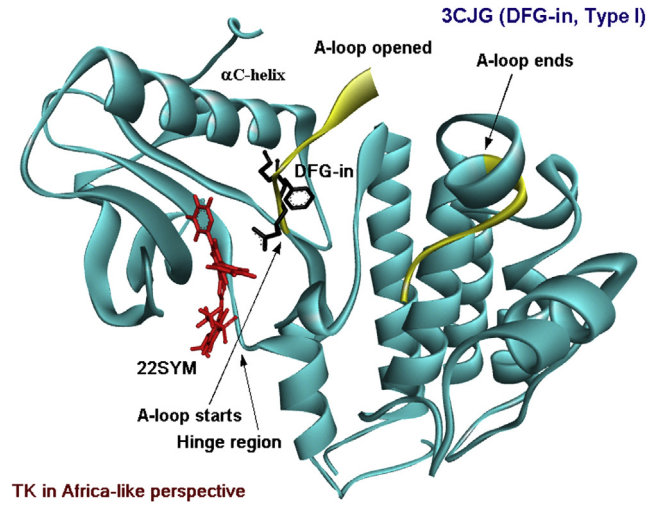

Fig. 8. An active VEGFR2 kinase from PDB: 3CJG (DFG-in, Type I ligand) with depicted DFG fragment on an A-loop and predicted pose for **22SYM** inhibitor. Phe residue from DFG fragment (in black) is oriented in an active kinase under the αC-helix situated almost horizontally in a left upper part of the protein structure (the kinase is shown in its "Africa-like" perspective: a complex with a hinge region on its down part showing a pose of **22SYM** ligand). Protein from PDB: 3CJG was superimposed [16] on the co-ordinates of VEGFR2 protein variant from PDB: 1Y6A complex possessing predicted pose of **22SYM** ligand.

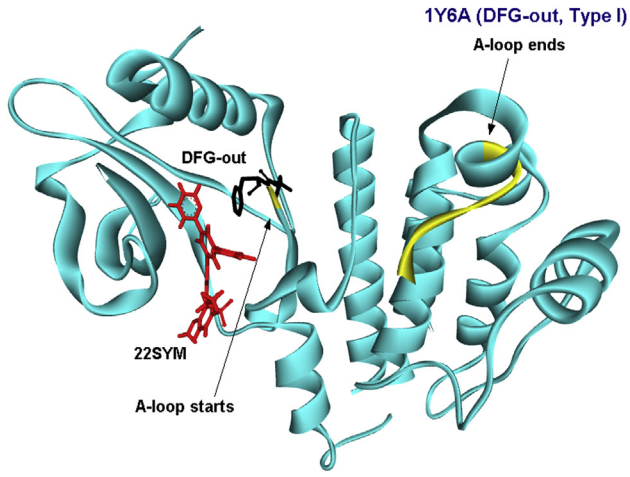

Fig. 9. The inactive (DFG-out) VEGFR2 kinase (PDB: 1Y6A) with A-loop DFG fragment (in black) and predicted pose of **22SYM** ligand (in red). In the above inactive kinase the Phe side chain residue from DFG fragment occupies a marginal part of the ATP binding pocket (For interpretation of the references to colour in this figure legend, the reader is referred to the web version of this article.).

The inactive (DFG-out) kinase form can be reached when DFG motif adopts a different conformation in which the DFG aspartate and phenylalanine side chains changes positions and point in opposite directions [14]. Based on 3D arrangement of 34 kinase DFG fragments we determined 30 variants of VEGFR2 TK in an inactive (DFG-out) conformation and only 4 kinases possessing an active (DFG-in) form (Table 3).

All available 34 PDB structures of VEGFR2 TK variants were divided into three main groups according to 3D arrangements of their DFG fragments:

1/**Active (DFG-in) VEGFR2 kinase variants** in PDB complexes: 1VR2 (no ligand present), 2P2H (ligand Type I), 3B8R (Type I 1/2) and 3CJG (Type I) do not have any direct collision of DFG fragment from their A-loop with **22SYM** in its predicted pose. Even though some controversial influence of an Asp1044 residue (from DFG fragment) positioned by the *U*-like pyridine group of **22SYM** can be considered. Both an electrostatic repulsion: Asp1044 residue/*U*-like pyridyl & an electrostatic attraction between negatively charged Asp1044 carboxylate and a protonated *U*-like pyridine in **22SYM** can be expected (Fig. 8).

2/**Inactive (DFG-out) VEGFR2 kinases PDB: 1Y6A**, **1Y6B and 3CJF** (all possessing Type I inhibitor) have an extraordinary 3D arrangement of their DFG fragments, that is not possible to find in any other of 31 VEGFR2 TK structures. All three protein variants from the above complexes are exceptional probably due to their surprisingly opened conformation of an A-loop that is not typical in inactive (PDB-out) kinases. From all of them the opened A-loop conformation is possible clearly observe only in a case of PDB: 3CJF (Fig. 11, the structure in the right). In the complex PDB: 3CJF only Asp1044 is visible from its DFG fragment. DFG fragments in PDB: 1Y6A and 1Y6B have no collisions with **22SYM** ligand (e.g. Fig. 9). In these cases, Phe1045 residue from DFG fragment beside common Π, Π interaction can provide also +, Π interaction with protonated *S*-like pyridyl group from **22SYM** ligand (Fig. 3). Interactions between **22SYM**/Phe1045 can help to stabilize a DFG-out kinase conformation. The most of the A-loops in both PDB: 1Y6A and 1Y6B complexes are disordered (Fig. 9).

3/We studied also **remaining 27 VEGFR2 protein variants, all in an inactive DFG-out arrangement** possessing Type-II inhibitor (if not mentioned otherwise). In 24 from them: 2P2I; 2OH4; 2QU5; 2QU6; 3B8Q; 2RL5; 3BE2; 3CP9; 3CPB; 3CPC; 3DTW; 3EWH; 3EFL; 2XIR; 3VHE; 3U6J; 3VNT; 3VHK; 4AG8; 4AGC; 4AGD (Type I); 4ASD; 4ASE and 3VO3 the position of Phe from DFG fragment is in strong collision with predicted pose of **22SYM** ligand. The *U*-like pyridyl substituent from **22SYM** is located in a sugar/phosphate region where the DFG-out Phe side chain is positioned (Fig. 10). In two remaining complexes: 1YWN and 3VID (Type I) only Asp amino acid residue is visible from their DFG fragments. In these cases, Asp is in similar arrangement as was seen in the other 24 proteins mentioned above. In a protein from the complex PDB: 3C7Q (Type I) we expect slightly less severe collision with **22SYM** ligand due to a bit different position of Phe from its DFG fragment compare to the other above mentioned 26 protein variants.

A kinase activation loop (A-loop) can be generally defined as beginning with the conserved residues DFG (Asp-Phe-Gly) and ending at the APE (Ala-Pro-Glu) sequence [7,17]. A-loop consists in VEGFR2 TK from 30 AA residues (e.g. in PDB: 1Y6A, Asp1044–Glu1073). Initially we thought that an A-loop is turning round a DFG joint and 3D arrangement of the DFG fragment reflects information about the conformation of an A-loop useful to estimate its position especially in case when this loop is not visible in an X-ray structure. By comparison of several kinase complexes possessing Type I ligand we observed that an A-loop can adopt more conformations that are not necessarily in relation with DFG-out kinase arrangement.

Within VEGFR2 protein variants we found an example of two inactive (DFG-out) kinases both possessing Type I inhibitor with opposite position of their activation loop. Despite that, the both proteins represent inactive kinases, A-loop in PDB: 4AGD is closed and 3CJF complex has its A-loop opened (Fig. 11).

2.7. Analysis of other 417 PDB tyrosine kinases

Within our effort to find another example of a different conformation of an A-loop in DFG-out tyrosine kinases possessing Type I inhibitor, 417 different kinase complexes were selected from PDB database with similar DFG 3D arrangement to that of complex PDB: 1Y6A. Also in these cases, we were able to find the structures

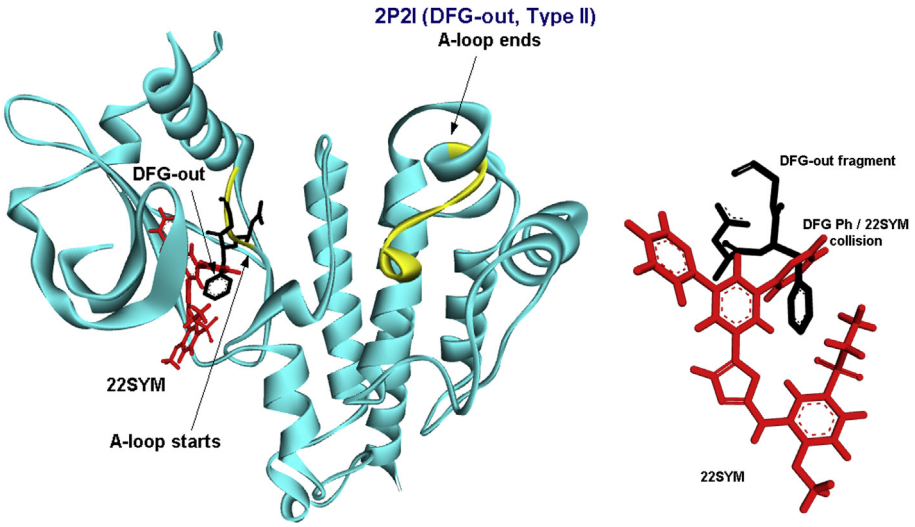

Fig. 10. In the left: a collision of the *U*-like pyridyl from **22SYM** ligand with Phe originating from DFG-out fragment of a VEGFR2 TK A-loop (PDB: 2P2I). The main part of an A-loop is not visible in this case. In the right: a detail of the severe collision of **22SYM** with the Phe residue from the A-loop DFG fragment. The protein from PDB: 2P2I was superimposed on coordinates of VEGFR2 variant from the complex PDB: 1Y6A possessing predicted pose of **22SYM** ligand.

of inactive tyrosine kinases (DFG-out, Type I) with oppositely oriented A-loops. Tyrosine kinase from a complex PDB: 3RHK (c-Met kinase) has its A-loop closed and a protein from a complex PDB: 1OPL (c-Abl kinase, similarly the others PDB: 1OPK, 1M52, 3UE4 and 2HZI) displays A-loop opened. In both cases (PDB: 3RHK and 1OPL), the whole A-loops are visible in their X-ray structures. In both kinases no phosphorylation on Tyr residues of their A-loops were present that means no influence of phosphorylation on the A-loop conformations (Fig. 12).

It is also interesting to note an example when two different VEGFR2 variants (both with Type I inhibitors) possesses similarly opened conformation of their A-loops: the inactive (DFG-out) PDB: 3CJF (Fig. 11, in the right)) and an active (DFG-in) PDB: 3CJG (Fig. 8). Both complexes have almost the same ligand, only the difference is N-methylation in case of PDB: 3CJG that forces the ligand to change its conformation compare to the one that is not methylated (in PDB: 3CJF). This is an interesting example confirming that the structure of the ligand can determine DFG-out or DFG-in kinase conformation. The above facts prove our observation that conformation of the A-loop (here opened in both cases) need not depend on the DFG arrangement (-out, or -in). An A-loop can be folded at different points not exclusively in a DFG joint (compare the A-loop shape close to the DFG fragment on Fig. 11 (the right structure) with one on Fig. 8 (their superimposition is not shown here)).

Table 1
Effects of **22SYM** on the proliferation of endothelial and tumour cells.

Cell line	IC_{50} [μM]
BAEC	0.37 ± 0.15
MDAMB231	3.99 ± 2.04
HT29	15.17 ± 2.33
HT1080	2.43 ± 2.10
HL60	17.83 ± 3.69
U2OS	2.03 ± 0.45

Results are expressed as IC_{50} (compound concentration, in μM, that causes 50% cell growth inhibition) and they are expressed as means ± S.D. of values of at least three independent experiments with triplicate samples each.

3. Conclusions

We developed chimeric VEGFR2 inhibitors **22SYM**, **23ASYM** and **33SYM** possessing two pyridyl substituents in one molecule mimicking the structure of both conformers of **AAZ** (PDB: 1Y6A) and/or their relative **AAX** ligand (PDB: 1Y6B). Bispyridyl compounds **22SYM**, **23ASYM**, **33SYM** bind selectively to VEGFR2 tyrosine kinase by concentration dependent manner. Their VEGFR2 enzymatic inhibition activities were determined together with reference compounds (**AAZ**, **sunitinib** and **sorafenib** salts) by a radiometric protein kinase assay. IC_{50} were found in a range from 15.1 10^{-9} M to 170 × 10^{-9} M. The most active compound **22SYM** (IC_{50} = 15.1 nM) possesses two pyrid-2-yl substituents in its structure. **22SYM** is a VEGFR2 TK (Type I) inhibitor with an enzymatic activity comparable or better to the clinical drugs Nexavar® (Bayer) and Sutent® (Pfizer) (Fig. 3). The most promising compound **22SYM** was screened by different *in vitro* and *in vivo* biological assays. We determined that **22SYM** selectively inhibits endothelial cells growth (IC_{50} = 370 nM), whereby five different tumour cells were used as well (Table 1). **22SYM** induces endothelial cells apoptosis at concentrations of 0.5 μM or higher (Fig. 4). **22SYM** at 1 μM concentration produces a significant inhibition of the migratory capability of endothelial cell (Fig. 5). **22SYM** at 1 μM concentration completely inhibits the endothelial cells capillary tube formation (Fig. 6). **22SYM** inhibits *in vivo* angiogenesis in the Zebrafish embryo assay at 20 μM on 87% (Fig. 7, Table 2). Embryo development was unaffected indicating a low toxicity of this compound. Even though the most interesting bispyridyl substance **22SYM** has only slightly better activity (IC_{50} = 15.1 nM) (Fig. 3) compare to an enzymatic activity of its relative **AAZ**

Table 2
Inhibition of *in vivo* angiogenesis by **22SYM**.

	22SYM (μM)	Positive/total	% Inhibition
Zebrafish assay	0	0/15	0
	5	1/15	7
	10	8/15	53
	20	13/15	87

Table 3
Thirty-four published VEGFR2 TK structures (1 protein and 33 protein complexes) are depicted in order as released in PDB database together with their properties like inhibitor Type classification, PDB code, DFG-in (active) or DFG-out (inactive) VEGFR2 TK conformation, a ligand abbreviation, Type classification, its activity or affinity if published in PDB, VEGFR2 TK primary structure mutation(s) when mentioned. Amino acid residue Val916 (in a wild type of hu-VEGFR2 TK) [15] represents a gatekeeper (sometimes referred as Val914 in complexes 1Y6A, 1Y6B, 1YWN, 2OH4, 3CJF, 3CJG). In 13 from 34 VEGFR2 complexes, the Valine gatekeeper was mutated to Threonine (V916T).

Released year in PDB	No of structures	PDB code[(DFG-in, -out descriptor)] (ligand identifier[(inhibitor type descriptor)] and VEGFR2 TK activity or affinity, mutation(s))
2000	1	1VR2[a] (VEGFR2 TK protein (no organic ligand included), mutation: E990V)
2005	3	1Y6A[b,h] (ligand identifier: AAZ[c], IC_{50}: 22 nM (VEGFR2 TK))
		1Y6B[b,h] (AAX[c], IC_{50}: 38 nM)
		1YWN[b,h] (LIF[e], IC_{50}: 3 nM, mutation: E990V)
2007	5	2P2H[a] (994[c], IC_{50}: 68 nM, mutations: C817A, V916T,[g] E990V)
		2P2I[b] (608[e], IC_{50}: 38 nM, K_i: 10 nM, mutations: C817A, E990V)
		2OH4[b,h] (GIG[e], IC_{50}: 3.5 nM, mutation: E990V)
		2QU5[b] (276[e], K_i: 8.7 nM, mutations: C817A, V916T,[g] E990V)
		2QU6[b] (857[e], IC_{50}: 4.6 nM, K_i: 2.8 nM, mutations: C817A, V916T,[g] E990V)
2008	11	3B8Q[b] (900[e], IC_{50}: 0.5 nM, mutations: C817A, V916T,[g] E990V)
		3B8R[a] (887[d], IC_{50}: 0.6 nM, mutations: C817A, V916T,[g] E990V)
		2RL5[b] (2RL[e], IC_{50}: 4 nM, mutations: C817A, V916T,[g] E990V)
		3BE2[b] (RAJ[e], IC_{50}: 2 nM, mutations: C817A, V916T,[g] E990V)
		3CP9[b] (C19[e], IC_{50}: 48 nM, mutations: C817A, V916T,[g] E990V)
		3CPB[b] (C92[e], IC_{50}: 25 μM, mutations: E817A, V916T,[g] E990V)
		3CPC[b] (C52[e], IC_{50}: 5 μM, mutations: C817A, V916T,[g] E990V)
		3DTW[b] (A96[e], IC_{50}: 353 nM, mutations: C817A, V916T,[g] E990V)
		3CJF[b,h] (SAV[c], IC_{50}: 6.3 nM)
		3CJG[a,h] (KIM[c])
		3C7Q[b] (XIN[c], IC_{50}: 21 nM)
2009	2	3EWH[b] (K11[e], IC_{50}: 69 nM, mutations: C817A, V916T,[g] E990V)
		3EFL[b] (706[e], IC_{50}: 3 nM, mutations: C817A, E990V)
2011	2	2XIR[b] (00J[e], mutation: yes, gatekeeper Val916 is preserved)
		3VHE[b] (42Q[e], IC_{50}: 6.2 nM, K_d: 19 nM)
2012	9	3U6J[b] (03X[e], mutations: V916T,[g] E990V)
		3VNT[b] (0JA[e])
		3VID[b] (4TT[c])
		3VHK[b] (BPK[f])
		4AG8[b] (AXI[e]: axitinib, mutation: yes, gatekeeper Val916 is preserved)
		4AGC[b,i] (AXI[e]: axitinib, mutation: yes, gatekeeper Val916 is preserved)
		4AGD[b] (B49[c]: sunitinib, mutation: yes, gatekeeper Val916 is preserved)
		4ASD[b] (BAX[e]: sorafenib, mutation: yes, gatekeeper Val916 is preserved)
		4ASE[b] (AV9[e]: tivozanib, mutation: yes, gatekeeper Val916 is preserved)
2013	1	3VO3[b] (0KF[e])

[a] An active (DFG-in) VEGFR2 tyrosine kinase variant (marked also by underlined PDB code in the table).
[b] VEGFR2 TK in an inactive (DFG-out) conformation.
[c] Type I inhibitor (marked also by underlined ligand code in the table).
[d] Type I 1/2 inhibitor (only in DFG-in kinases).
[e] Type II inhibitor (only in DFG-out kinases).
[f] Type III inhibitor (out of an ATP binding side).
[g] Gatekeeper amino acid residue mutation.
[h] Primary amino acid numbering shifted at -2 compare to the wild type hu-VEGFR2 described in Ref. [15].
[i] Similar to komplex 4AG8 + juxtamembrane domain (Tyr801-Pro812).

ligand (IC_{50} = 17.1 nM) that is in contrary with expectation based on our in Silico prediction.

We analysed all 34 VEGFR2 TK variants (Table 3) and other 417 tyrosine kinase structures available in PDB in order to explain this discrepancy. We found that inactive tyrosine kinase complexes both possessing Type I ligands and DFG-out arrangement can surprisingly adopt opposite conformations of their A-loop (Table 4).

Based on the above analyses we proposed that the activation loops (A-loops), in inactive (DFG-out) tyrosine kinases possessing Type I inhibitor, are not stabilized enough and can change their conformations e.g. from the opened (PDB: 3CJF, 1OPL) to the closed ones (PDB: 4AGD, 3RHK) (Table 4) independently on kinase DFG arrangement. Therefore, the activity of Type I inhibitors bound in DFG-out VEGFR2 variants, especially inhibitors that has a part of its structure oriented towards an A-loop (e.g. **22SYM**), can be influenced due to the collisions between an inhibitor and some part from the dynamically moving A-loop. Observed averaged activity of **22SYM** VEGFR2 inhibitor can be lowered compare to the expecting one due to the collisions between the *U*-like pyridyl group of **22SYM** and Ph residue from a DFG fragment of a kinase A-loop (Fig. 10). This can result in only slightly better activity of **22SYM** inhibitor (IC_{50} = 15.1 nM, predicted docking score: −60.1 kcal/mol) compare to an enzymatic activity of its relative **AAZ** ligand (IC_{50} = 17.1 nM, predicted docking score: −52.9 kcal/mol) that is in contrary with our expectations based on the docking experiment at the beginning of our research.

The above features should be considered before a development of Type I tyrosine kinase inhibitors that partially occupy the possible position of a flexible A-loop in DFG-out tyrosine kinases.

4. Experimental

4.1. Docking

Docking experiments were accomplished according to the expert self-assessing system DOCK Blaster [18]. Calculations were based on DOCK 3.6 a version of UCSF DOCK software [19].

4.2. Synthesis

4.2.1. General

^1H and ^{13}C NMR spectra were recorded on Varian Gemini (300 MHz and 75 MHz, resp.) using tetramethylsilane as an internal standard. IR spectra were acquired on FT-IR-ATR REACT IR 1000 (ASI

Applied Systems) with diamond probe and MTS detector. The progress of reactions was followed by TLC analysis (Merck Silica gel 60 F_{254}). UV lamp (254 nm) and iodine vapours were used for spots visualization. Silica gel Merck 60 (40–63 μm) was used for FLC. Melting points were determined by Kofler apparatus or Barnstead Electrothermal IA9200 and are uncorrected. Elemental analyses were carried out on Vario MICRO Cube apparatus. 1-(4-Aminophenyl)ethanone (**1**) was purchased from Sigma–Aldrich company. Some solvents abbreviations used in experimental part are as follows: AN (acetonitrile), DCM (dichloromethane), DME (1,2-dimethoxyethane), EA (ethyl acetate), Hex (nonpolar mixture of hexanes). Other used abbreviations: FLC (Flash Liquid Chromatography), RVE (Rotary Vacuum Evaporator), HV (High Vacuum, ca 0.03 Torr).

4.2.2. 1-(4-Amino-3,5-dibromophenyl)ethanone (**2**)

A half volume of a solution 21.6 ml (67.12 g, 420.0 mmol, 2.00 mol eq) Br_2 in 50 ml AcOH conc. was added dropwise by stirring to a solid starting material 28.38 g (210.0 mmol, 1.00 mol eq) 1-(4-aminophenyl)ethanone (**1**) within 20 min at rt. Then 30 ml of water was added to the reaction at once. The second volume of the above bromine solution in AcOH was added dropwise to the reaction mixture within another 20 min. Afterwards another portion of water (20 ml) was added. The final mixture was stirred at 45 °C for 20 min. Afterwards 30 ml of water was added and the mixture was allowed to cool to rt. The precipitated solid material was filtered off, washed with 3 × 50 ml of cold water and dried on the air. The crude product 45.70 g (156.0 mmol, 74.0%) **2** was obtained as a white solid material and purified by crystallization from EtOH. Mp: 162.0–164.0 °C [EtOH], lit: 168.0–169.0 °C [EtOH] [20] IR ν (solid, cm^{-1}): 3471 (m, N–H), 3353 (m, N–H), 3079 (m), 1664 (s, C=O), 1598 (s), 1531 (m), 1401 (m), 1355 (m), 1311 (m), 1253 (m), 1231 (m), 873 (m), 716 (m). ^{1}H NMR (300 MHz, $CDCl_3$): δ 8.01 (s, 2H, H–C(2)), 5.06 (br s, 2H, $-NH_2$), 2.50 (s, 3H, $-COCH_3$) [21]. ^{13}C NMR (75 MHz, $CDCl_3$) δ: 194.2 (C=O), 145.9C(4), 133.2 C(2), 132.5 C(1), 107.7 C(3), 26.0 (CH_3) [21]. Anal. calcd. for $C_8H_7Br_2NO$ (292.96): C, 32.80; H, 2.41; Br, 54.55; N, 4.78; found: C, 32.39; H, 2.15; Br, 54.09; N, 4.53.

4.2.3. 1-(3,5-Dibromophenyl)ethanone (**3**)

To a suspension of 45.00 g (153.6 mmol, 1.00 mol eq) 1-(4-amino-3,5-dibromo-phenyl)ethanone (**2**) in 160 ml of benzene and 950 ml of EtOH 38.5 ml of conc. H_2SO_4 was added dropwise (ca 15 min) so that the temperature of the reaction mixture was not allowed to rise over 50 °C. Afterwards the mixture was refluxed for 30 min, it was cooled to 10 °C and 6.00 g (94.4 mmol, 0.61 mol eq) copper powder was added portionwise within 20 min. The mixture was cooled to 0 °C. The solution of 28.00 g (405.8 mmol, 2.64 mol eq) $NaNO_2$ in 40 ml of water was added slowly to the reaction mixture. The mixture was left to stand at rt for 12 h. After this time, the mixture was refluxed for 3 h, cooled to 40 °C and the formed solid material was filtered off and washed with cold ethanol. The solution obtained after filtration was evaporated to a half volume and extracted with 40 ml of $CHCl_3$. The organic layer was separated

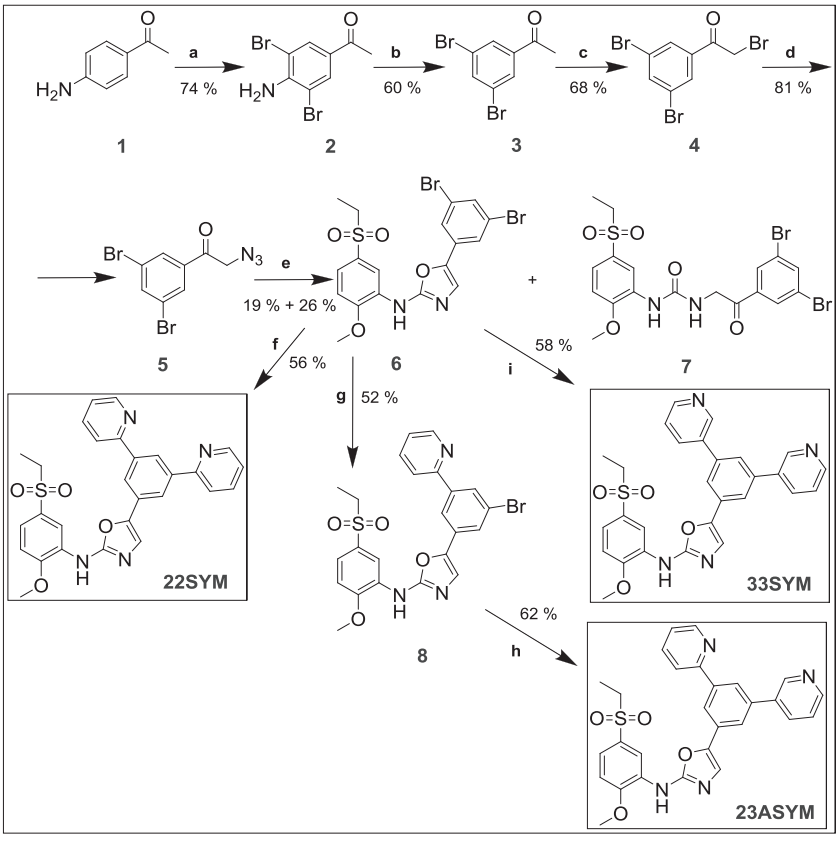

Scheme 1. Preparation of predicted compounds **22SYM**, **23ASYM**, **33SYM** was performed in six or seven synthetic steps starting from commercially available *p*-aminoacetophenone (**1**). The reaction conditions are as follow: [a]/Br_2, AcOH, H_2O, rt to 45 °C; yield 74% (**2**); [b]/1/H_2SO_4 conc., PhH, EtOH, reflux; 2/$NaNO_2$, Cu powder, 12 h, rt, than reflux 3 h; yield 60% (**3**); [c]/Br_2, Et_2O, 8 h, rt; yield 68% (**4**); [d]/NaN_3, MeOH, 0 °C, 2.5 h; yield 81% (**5**); [e]/4-(ethylsulfonyl)-2-isocyanato-1-methoxybenzene (**5b**) prepared from **5a** by $COCl_2$, PPh_3, DCM, 1 h, rt; yield 19% (**6**) and 26% (**7**); [f]/Bu_4NBr, $(PPh_3)_4Pd$, py-2-ylSnBu$_3$ (2.5 mol eq), AN, Ar, sealed tube, 100 °C, 48 h; yield 56% (**22SYM**); [g]/Bu_4NBr, $(PPh_3)_4Pd$, py-2-ylSnBu$_3$ (1.0 mol eq), AN, Ar, sealed tube, 100 °C, 48 h; yield 52% (**8**); [h]/Bu_4NBr, $(PPh_3)_4Pd$, py-3-ylSnBu$_3$ (1.0 mol eq), AN, Ar, sealed tube, 100 °C, 48 h; yield 62% (**23ASYM**); [i]/$(PPh_3)_4Pd$, py-3-ylB(HO)$_2$, DME, Na_2CO_3, Ar, sealed tube, reflux, 1 h; yield 58% (**33SYM**).

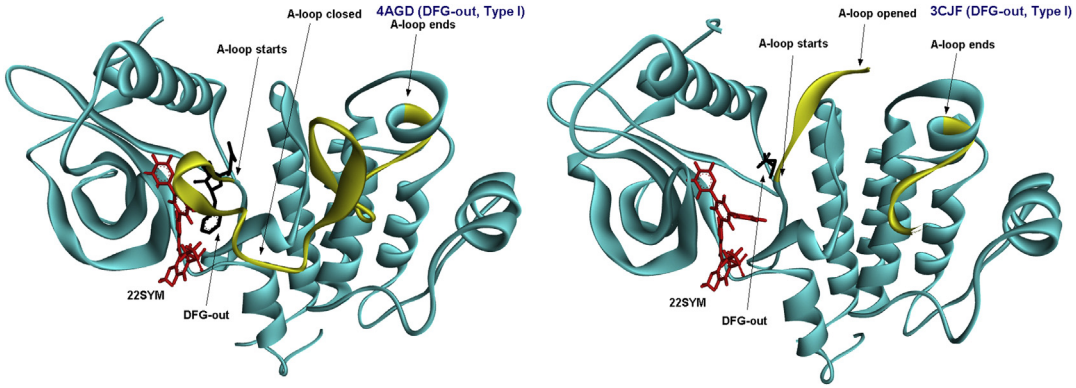

Fig. 11. In the left: PDB: 4AGD (DFG-out kinase, Type I inhibitor) with VEGFR2 protein variant possesses a closed activation loop (in this case less important amino acid residues 802–812 were hidden for clarity). In the right: a protein variant from PDB: 3CJF (DFG-out, Type I inhibitor) possesses an open-like activation loop. In this case only Asp from DFG triad is visible. Both A-loops are marked yellow. Both proteins were superimposed on the coordinates of VEGFR2 protein from PDB: 1Y6A possessing predicted pose of **22SYM** ligand (For interpretation of the references to colour in this figure legend, the reader is referred to the web version of this article.).

and the water layer extracted with $CHCl_3$ (2 × 80 ml). The combined organic layer was washed twice with water (2 × 70 ml) and dried by standing over Na_2SO_4, filtered and evaporated on RVE. The crude oil was crystallized from MeOH to yield 25.80 g (92.8 mmol, 60.0%) of required product **3**. Mp: 61.0–63.0 °C [MeOH]. Lit: 61.0–63.0 °C [EtOH aq] [22]. IR ν (solid, cm^{-1}): 3073 (w), 2920 (w), 1693 (s, C=O), 1558 (s), 1410 (m), 1356 (m), 1244 (m), 670 (m). ^1H NMR (300 MHz, $CDCl_3$): δ 8.00 (d, 2H, J(2,4) = 1.8 Hz, H–C(2)), 7.86 (t, 1H, J(2,4) = 1.8 Hz, H–C(4)), 2.59 (s, 3H, CH_3). ^{13}C NMR (75 MHz, $CDCl_3$): δ 195.2 (C=O), 139.8C(4), 138.2 C(1), 130.1 C(2), 123.5 C(3), 26.6 (CH_3) [18]. Anal. calcd. for $C_8H_6Br_2O$ (277.94): C, 34.57; H, 2.18; Br, 57.50; found: C, 34.42; H, 2.04; Br, 57.63.

4.2.4. 2-Bromo-1-(3,5-dibromophenyl)ethanone (*4*)

Bromine 200 μl (620.6 mg, 3.88 mmol, 1.08 mol eq) was added dropwise at rt to the solution of 1.00 g (3.60 mmol, 1.00 mol eq) 1-(3,5-dibromophenyl)ethanone (**3**) in 15 ml of Et_2O within 15 min. The reaction mixture was stirred 8 h at rt until the colour of bromine disappeared. The reaction mixture was treated with 10% aqueous solution of $Na_2S_2O_3$ to get rid of the traces of unreacted bromine. The organic layer was separated and the water layer extracted with Et_2O (3 × 15 ml). The combined organic layers were dried by standing over an anhydrous Na_2SO_4, filtered, solution evaporated on RVE and dried by HV. The crude mixture (1.26 g, contained small amount of dibrominated product) was crystallized from Et_2O/Hex. The desired product **4** was obtained as a yellow powder in 870 mg (2.44 mmol, 68.0%). Mp: 78.0–83.0 °C [Et_2O/Hex], lit: 85.0–86.0 °C [EtOH] [23]. IR ν (solid, cm^{-1}): 3080 (m, aromatic C–H), 2997 (m, aliphatic C–H), 1700 (s, C=O), 1552 (s), 1408 (s), 1382 (m), 1188 (s), 1158 (m), 736 (s). ^1H NMR (300 MHz, $CDCl_3$): δ 8.03 (d, 2H, J(2,4) = 1.8, H–C(2)), 7.90 (t, 1H, J(2,4) = 1.8, H–C(4)), 4.38 (s, 2H, $-COCH_2Br$) [23]. ^{13}C NMR (75 MHz, $CDCl_3$): δ 188.8 (C=O), 139.1C(4), 136.6 C(1), 130.6 C(2), 123.7 C(3), 29.3 ($-CH_2Br$) [23]. Anal. calcd. for $C_8H_5Br_3O$ (356.84): C, 26.93; H, 1.41; Br, 67.18; found: C, 26.63; H, 1.38; Br, 67.06%.

4.2.5. 2-Azido-1-(3,5-dibromophenyl)ethanone (*5*)

Sodium azide 73.0 mg (1.12 mmol, 2.00 mol eq) was added portionwise to a solution of 200.0 mg (0.56 mmol, 1.00 mol eq) 2-bromo-1-(3,5-dibromophenyl)ethanone (**4**) in 4 ml of MeOH at 0 °C within 1.5 h. The mixture was stirred for another 1 h at 0 °C. Later the reaction was poured into 18 ml of water with crushed ice. Initially formed emulsion solidified at 0 °C after 1 h. The crude material was filtered off and washed with cold water. Then the crude product was dissolved in Et_2O and solution was dried over Na_2SO_4, filtered and evaporated. The product 145.0 mg (0.45 mmol, 81.0%) **5** was obtained as an orange powder. Mp: 73.0–74.0 °C. IR ν (solid, cm^{-1}): 3074 (m), 2917 (m), 2104 (m, N_3), 1693 (s, C=O), 1614 (m), 1544 (m), 1410 (m), 1363 (m), 1249 (m), 1208 (s), 740 (w). ^1H NMR (300 MHz, $CDCl_3$): δ 7.96 (d, 2H, J(2,4) = 1.8, H–C(2)), 7.92 (t,

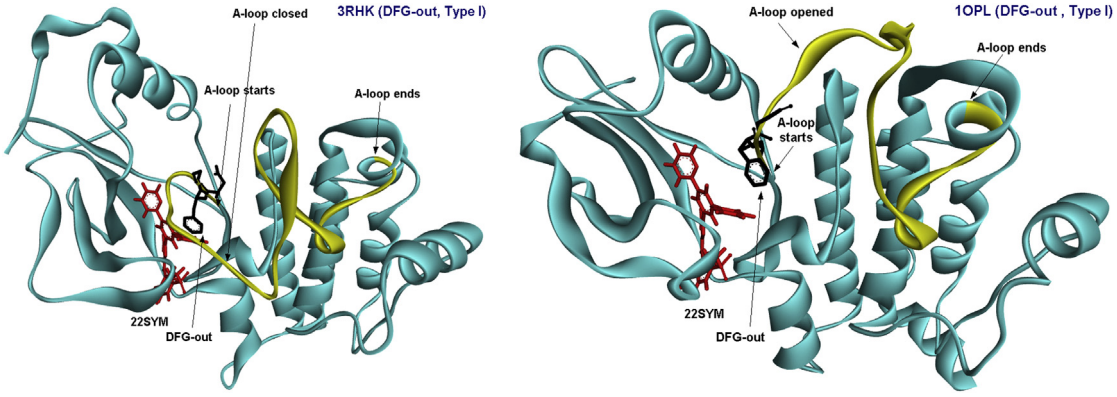

Fig. 12. An example of the oppositely positioned flexible tyrosine kinase activation loops in different tyrosine kinases, both in an inactive DFG-out conformation, possessing Type I inhibitor. In the left: c-Met kinase (PDB: 3RHK) with a closed activation loop (Asp1222–Glu1253). In the right: c-Abl kinase (PDB: 1OPL) with an opened activation loop (Asp400–Glu428) (myristic acid from a complex 1OPL was omitted for clarity). Both proteins were superimposed on the coordinates of VEGFR2 protein from PDB: 1Y6A possessing predicted pose of **22SYM** ligand.

Table 4
Selected inactive tyrosine kinase complexes possessing Type I ligand demonstrating independence of an A-loop conformation (closed or opened) on a preserved DFG-out kinase arrangement.

PDB: 4AGD (VEGFR2 kinase)	PDB: 3CJF (VEGFR2 kin.)	PDB: 3RHK (c-Met kin.)	PDB: 1OPL (c-Abl kin.)
Type I	Type I	Type I	Type I
DFG-out	DFG-out	DFG-out	DFG-out
A-loop closed	**A-loop opened**	**A-loop closed**	**A-loop opened**
Fig. 11, left part	Fig. 11, right part	Fig. 12, left part	Fig. 12, right part

1H, *J*(2,4) = 1.8, H–C(4)), 4.51 (s, 2H, $-CH_2N_3$). ^{13}C NMR (75 MHz, $CDCl_3$): δ 190.9 (C=O), 139.3C(4), 136.9 C(1), 129.7 C(2), 123.9 C(3), 54.9 ($-CH_2N_3$). Anal. calcd. for $C_8H_5Br_2N_3O$ (318.95): C, 30.13; H, 1.58; Br, 50.10; N, 13.17; found: C, 30.05; H, 1.48; Br, 50.23; N, 12.70.

4.2.6. 4-(Ethylsulfonyl)-2-isocyanato-1-methoxybenzene (**5b**)

Recently we have described the synthesis of 5-(ethylsulfonyl)-2-methoxyaniline (**5a**) from commercially available 4-methoxybenzenesulfonyl chloride (or anisole) [12]. 4-(Ethylsulfonyl)-2-isocyanato-1-methoxybenzene (**5b**) was prepared from 5-(ethylsulfonyl)-2-methoxyaniline (**5a**) by heating of 500 mg (2.30 mmol, 1.00 mol eq) **5a** in 10 ml of toluene (abs) with 4.0 ml (5.25 mmol, 3.20 mol eq, 20% w/w $COCl_2$ in toluene) phosgene solution to reflux within 3 h. Subsequently the reaction mixture was worked up by RVE evaporation. The product was obtained as brown solid 504 mg (2.25 mmol, 97.8%). Mp: 101.8–104.3 °C. IR ν (solid, cm^{-1}): 3017 (w), 2868 (m), 2264 (w), 1603 (s), 1451 (m), 1308 (s, S=O), 1260 (s), 1123 (s, S=O), 1044 (s), 737 (m). ^{1}H NMR (300 MHz, $CDCl_3$): δ 7.74 (dd, 1H, *J*(5,6) = 8.7 Hz, *J*(3,5) = 2.3 Hz, H–C(5)), 7.53 (d, 1H, *J*(3,5) = 2.3 Hz, H–C(3)), 7.37 (d, 1H, *J*(5,6) = 8.7 Hz, H–C(6)), 4.04 (s, 3H, $-OCH_3$), 3.27 (q, 2H, *J*(CH_2,CH_3) = 7.4 Hz, SO_2CH_2), 1.08 (t, 3H, *J*(CH_3,CH_2) = 7.4 Hz, $SO_2CH_2\underline{CH_3}$). ^{13}C NMR (75 MHz, DMSO-d_6): δ 152.3 (N=*C*=O), 151.5 (C1), 130.0 (C2), 129.0 (C4), 122.5 (C5), 117.3 (C3), 110.8 (C6), 56.3 ($-OCH_3$), 49.6 (SO_2CH_2), 7.3 ($SO_2CH_2\underline{CH_3}$). An. calcd. for $C_{10}H_{11}NO_4S$ (241.26): C, 49.78; H, 4.60; N, 5.81; S, 13.29; found: C, 49.82; H, 4.65; N, 5.75; S, 13.24.

4.2.7. 5-(3,5-Dibromophenyl)-N-[5-(ethylsulfonyl)-2-methoxyphenyl]oxazol-2-amine (**6**)

A solution of 261.0 mg (1.00 mmol, 1.00 mol eq) PPh_3 in 5 ml of DCM was added portionwise (within 2 h) in a solution of 320.0 mg (1.00 mmol, 1.00 mol eq) 2-azido-1-(3,5-dibromophenyl)ethanone (**5**) and 241.2 mg (1.00 mmol, 1.00 mol eq) of 4-(ethylsulfonyl)-2-isocyanato-1-methoxybenzene (**5b**) in 5 ml of DCM at 0 °C over 1 h. Afterwards the reaction mixture was stirred 1 h at rt. Then 5 ml of hexanes was added to the reaction mixture and polar oil was formed due to its insolubility. The oil was separated by decantation. The product **6** 100.0 mg (0.194 mmol, 19.1%) was obtained from the oil by flash chromatography on silica with eluent Hex : EA (1:1). Mp: 231.0–233.0 °C [FLC]. IR ν (solid, cm^{-1}): 3414 (m, NH), 3026 (w), 2854 (w), 1601 (s), 1574 (s), 1549 (s), 1527 (m), 1429 (m), 1308 (s, S=O), 1264 (s), 1123 (s, S=O), 1020 (s), 737 (m). ^{1}H NMR (300 MHz, DMSO-d_6): δ 8.85 (d, 1H, *J*(4,6) = 2.3 Hz, H–C(6)), 7.66 (br s, 1H, –NH–), 7.61 (d, 2H, *J*(2′,4′) = 1.6 Hz, H–C(2′)), 7.58 (dd, 1H, *J*(3,4) = 8.6, *J*(4,6) = 2.3 Hz, H–C(4)), 7.52 (t, 1H, *J*(2′,4′) = 1.6 Hz, H–C(4′)), 7.23 (s, 1H, H–$C(4_{ox})$), 7.01 (d, 1H, *J*(3,4) = 8.6 Hz, H–C(3)), 4.03 (s, 3H, $-OCH_3$), 3.17 (q, 2H, *J*(CH_2, CH_3) = 7.4 Hz, $-OCH_2-$), 1.32 (t, 3H, *J*(CH_2, CH_3) = 7.4 Hz, $-CH_3$). ^{13}C NMR (75 MHz, DMSO-d_6): δ 155.6 ($C2_{ox}$), 150.5 (C2), 142.6 ($C5_{ox}$), 132.5 (C5), 131.0 (C1), 130.9 (C2′), 128.4 (C4′), 124.5 (C1′), 124.2 (C4), 123.5 (C3′), 122.9 ($C4_{ox}$), 115.6 (C6), 109.6 (C3), 56.3 ($-OCH_3$), 50.7 ($-SO_2CH_2-$), 7.6 ($-SO_2CH_2\underline{C}H_3$). Anal. calcd. for $C_{18}H_{16}Br_2N_2O_4S$ (516.20): C, 41.88; H, 3.12; Br, 30.96; N, 5.43; S, 6.21; found: C, 41.62; H, 2.86; Br, 31.32; N, 4.99; S, 6.03.

4.2.8. 1-[2-(3,5-dibromophenyl)-2-oxoethyl]-3-[5-(ethylsulfonyl)-2-methoxyphenyl]urea (**7**)

The side product **7** 139.0 mg (0.261 mmol, 26.0%) was obtained by column chromatography of the crude reaction mixture obtained by synthesis of oxazole **6**, (silica, Hex:EA; 1:1). Mp: 149.0–153.0 °C [FLC]. IR ν (solid, cm^{-1}): 3325 (m, NH), 3072 (w), 2940 (w), 1744 (s, C=O), 1654 (s, C=O), 1594 (s), 1524 (s), 1411 (s), 1370 (m), 1305 (s, S=O), 1260 (s), 1228 (s), 1130 (s, S=O), 1084 (m), 1019 (w), 836 (w), 815 (w), 774 (w), 738 (m). ^{1}H NMR (300 MHz, $CDCl_3$): δ 8.13 (s, 1H, –Ar*NH*CO–), 7.95 (d, 1H, *J*(4,6) = 2.3 Hz, H–C(6)), 7.83 (dd, 1H, *J*(3,4) = 8.7, *J*(4,6) = 2.3 Hz, H–C(4)), 7.67 (d, 2H, *J*(2′,4′) = 1.7 Hz, H–C(2′)), 7.58 (t, 1H, *J*(2′,4′) = 1.6 Hz, H–C(4′)), 7.02 (d, 1H, *J*(3,4) = 8.7 Hz, H–C(3)), 6.11 (t, 1H, *J*(NH,CH_2) = 4.5 Hz, –CO*N*HCH_2–), 4.70 (d, 2H, *J*(NH,CH_2) = 4.5 Hz, CONHCH_2), 3.87 (s, 3H, $-OCH_3$), 3.08 (q, 2H, *J*(CH_2,CH_3) = 7.5 Hz, $-CH_2-$), 1.21 (t, 3H, *J*(CH_2,CH_3) = 7.5 Hz, $-CH_3$). ^{13}C NMR (75 MHz, DMSO-d_6): δ 189.3 (–CH_2*C*O–), 156.3 (–NH*C*ONH–), 154.3 (C2), 139.1 (C1′), 134.3 (C5), 130.8 (C2′), 130.1 (C1), 128.3 (C4′), 123.4 (C3′), 121.2 (C4), 116.2 (C6), 111.0 (C3), 56.3 (–OMe), 50.6 ($-SO_2CH_2CH_3$), 45.8 ($-CH_2$CO–), 7.6 ($-SO_2CH_2CH_3$). Anal. calcd. for $C_{18}H_{18}Br_2N_2O_5S$ (534,22): C, 40.47; H, 3.40; Br, 29.91; N, 5.24; S, 6.00; found: C, 40.27; H, 3.19; Br, 29.89; N, 5.41; S, 6.10.

4.2.9. 5-[3,5-Di(pyridin-2-yl)phenyl]-N-[5-(ethylsulfonyl)-2-methoxyphenyl]oxazol-2-amine (**22SYM**)

A mixture of 50.0 mg (0.097 mmol, 1.00 mol eq) 5-(3,5-dibromophenyl)-*N*-[5-(ethylsulfonyl)-2-methoxyphenyl]oxazol-2-amine (**6**), 47.0 mg (0.146 mmol, 1.50 mol eq) tetrabutylammonium bromide, 7.0 mg (0.006 mmol, 0.06 mol eq) tetrakis(-triphenylphosphine)palladium(0), 89.0 mg (0.242 mmol, 2.49 mol eq) 2-(tributylstannyl)pyridine and 1 ml of AN abs was sealed under Ar in a dry glass Pasteur tube and heated at 100 °C for 48 h. Then, after cooling, the tube was opened and its content poured into 25 ml of EA and 10 ml of 1 M water solution of KF was added. The mixture was stirred 3 h at rt. The organic layer was separated and the water layer extracted 3 × 25 ml of EA. The combined organic layer was dried by standing over Na_2SO_4, filtered and evaporated by RVE and HV to dryness. The solid material was separated by FLC (SiO_2, EA:Hex (2:1)). The product 28.0 mg (0.055 mmol, 56.3%) **22SYM** was obtained as a white powder. Mp: 255.0–257.0 °C [EtOH]. IR ν (solid, cm^{-1}): 3416 (m, NH), 3186 (m), 2937 (m), 1610 (s), 1578 (s), 1521 (m), 1429 (m), 1300 (s, S=O), 1261 (s), 1121 (s, S=O), 1020 (s), 716 (m). ^{1}H NMR (300 MHz, DMSO-d_6): δ 9.94 (s, 1H, NH), 8.84 (d, 1H, *J*(4,6) = 2.2 Hz, H–C(6), 8.75 (ddd, 1H, *J*(5″,6″) = 4.7 Hz, *J*(4″,6″) = 1.8 Hz, *J*(3″,6″) = 0.9 Hz, H–C(6″)), 8.67 (t, 1H, *J*(2′,4′) = 1.6 Hz, H–C(4′)), 8.44 (d, 2H, *J*(2′,4′) = 1.6 Hz, H–C(2′)), 8.18 (ddd, 1H, *J*(3″,4″) = 7.9 Hz, *J*(3″,5″) = *J*(3″,6″) = 0.9 Hz, H–C(3″)), 7.98 (ddd, 1H, *J*(3″,4″) = 7.9 Hz, *J*(4″,5″) = 7.6 Hz, *J*(4″,6″) = 1.8 Hz, H–C(4″)), 7.79 (s, 1H, H–$C(4_{ox})$), 7.51 (dd, 1H, *J* (3,4) = 8.6 Hz, *J*(4,6) = 2.2 Hz, H–C(4)), 7.45 (ddd, 1H, *J*(4″,5″) = 7.6 Hz, *J*(5″,6″) = 4.7 Hz, *J*(3″,5″) = 0.9 Hz, H–C(5″)), 7.29 (d, 1H, *J*(3,4) = 8.6 Hz, H–C(3)), 4.01 (s, 3H, $-OCH_3$), 3.22 (q, 2H, = 7.4 Hz, $-CH_2-$), 1.13 (t, 3H, *J*(CH_2,CH_3) = 7.4 Hz, $-CH_3$). ^{13}C NMR (75 MHz, DMSO-d_6): δ 156.6 (C2″), 155.3 ($C2_{ox}$), 150.5 (C2), 149.7 (C6″), 145.4 ($C5_{ox}$), 140.6 (C3′), 137.0 (C4″), 132.0 (C5), 131.0 (C1), 128.6 (C1′), 124.4 (C4′), 122.7 ($C4_{ox}$), 122.6 (C3″), 122.5 (C4), 122.0 (C2′), 120.9 (C5″), 115.3 (C6), 109.5 (C3), 56.3 (-OCH_3), 50.7 ($-CH_2-$), 7.6 (-CH_3). Anal. calcd. For $C_{28}H_{24}N_4O_4S$ (512.58): C, 65.61; H, 4.72; N, 10.93; S, 6.26; found: C, 65.58; H, 4.58; N, 10.78; S, 6.07.

4.2.10. 5-[3,5-Di(pyridin-3-yl)phenyl]-N-[5-(ethylsulfonyl)-2-methoxyphenyl]oxazol-2-amine (**33SYM**)

A mixture of 110.0 mg (0.213 mmol, 1.00 mol eq) 5-(3,5-dibromophenyl)-*N*-[5-(ethylsulfonyl)-2-methoxyphenyl]oxazol-2-amine (**6**), 6.0 mg (0.005 mmol, 0.024 mol eq) tetrakis(-triphenylphosphine)palladium(0) in 5 ml of 1,2-dimethoxyethane was stirred at rt within 10 min. Then a solution of 60.0 mg (0.49 mmol, 2.29 mol eq) 3-pyridinylboronic acid in 2 ml of 1 M aqueous Na_2CO_3 was added and the reaction mixture was gently refluxed within 1 h. The mixture was cooled to rt and 30 ml of water was added. After separation of organic layer, the water solution was extracted 3 × 5 ml of $CHCl_3$. The combined organic layer was extracted with 5 ml of 1 M Na_2CO_3 aqueous solution, dried by standing over Na_2SO_4, filtered and the solvent was removed by RVE and HV. The crude mixture was separated by FLC (silica, MeOH : EA (1:3)). The product 63.0 mg (0.123 mmol, 57.8%) **33SYM** was obtained as white powder. Mp: 206.0–207.0 °C [FLC]. IR ν (solid, cm^{-1}): 3426 (m, NH), 2924 (m), 2852 (m), 1613 (s), 1553 (s), 1524 (m), 1430 (m), 1301 (s, S=O), 1264 (s), 1122 (s, S=O), 1022 (s), 706 (m). ^{1}H NMR (300 MHz, DMSO-d_6): δ 8.96 (d, 1H, J(2″,4″) = 2.0 Hz, H–C(2″)), 8.88 (d, 1H, J(4,6) = 2.2 Hz, H–C(6)), 8.62 (dd, 1H, J(5″,6″) = 5.0 Hz, J(4″,6″) = 1.8 Hz, H–C(6″)), 8.06 (ddd, 1H, J(4″,5″) = 7.9 Hz, J(2″,4″) = 2.0 Hz, J(4″,6″) = 1.8 Hz, H–C(4″)), 7.81 (d, 2H, J(2′,4′) = 1.6 Hz, H–C(2′)), 7.72 (s, 1H, NH), 7.67 (t, 1H, J(2′,4′) = 1.6 Hz, H–C(4′)), 7.60 (dd, 1H, J(3,4) = 8.5 Hz, J(4,6) = 2.2 Hz, H–C(4)), 7.48 (dd, 1H, J(4″,5″) = 7.9 Hz, J(5″,6″) = 5.0 Hz, H–C(5″)), 7.36 (s, 1H, H–C(4_{ox})), 7.04 (d, 1H, J(3,4) = 8.5 Hz, H–C(3)), 4.05 (s, 3H, –OCH_3), 3.17 (q, 2H, J(CH_2,CH_3) = 7.5 Hz, –CH_2–), 1.30 (t, 3H, J(CH_2,CH_3) = 7.5 Hz, –CH_3). ^{13}C NMR (75 MHz, DMSO-d_6): δ 155.5 ($C2_{ox}$), 150.5 (C2), 148.9 (C2″), 148.0 (C6″), 144.8 ($C5_{ox}$), 139.5 (C3′), 135.9 (C4″), 134.9 (C3″), 131.0 (C1), 129.7 (C5), 128.7 (C1′), 124.9 (C4′), 123.9 (C2′), 123.2 ($C4_{ox}$), 122.8 (C4), 121.4 (C5″), 115.4 (C6), 109.5 (C3), 56.4 (-OCH_3), 50.7 (–CH_2–), 7.6 (–CH_3). Anal. calcd. for $C_{28}H_{24}N_4O_4S$ (512.58): C, 65.61; H, 4.72; N, 10.93; S, 6.26; found: C, 65.23; H, 4.58; N, 10.79; S, 6.16.

4.2.11. 5-[3-Bromo-5-(pyridin-2-yl)phenyl]-N-[5-(ethylsulfonyl)-2-methoxyphenyl]oxazol-2-amine (**8**)

A mixture of 50.0 mg (0.097 mmol, 1.00 mol eq) 5-(3,5-dibromophenyl)-*N*-[5-(ethylsulfonyl)-2-methoxyphenyl]oxazol-2-amine (**6**), 31.0 mg (0.096 mmol, 1.00 mol eq) tetrabutylammonium bromide, 7.0 mg (0.0061 mmol, 0.063 mol eq) tetrakis(-triphenylphosphine)palladium(0), 36.0 mg (0.097 mmol, 1.00 mol eq) 2-(tributylstannyl)pyridine in 1 ml of AN was sealed in a dry glass Pasteur tube under Ar. The reaction mixture was stirred and heated at 100 °C for 48 h. Then the tube was opened and the mixture poured into 25 ml of EA and 10 ml of 1 M aqueous solution of KF. The mixture was stirred for 3 h at rt. The organic layer was separated and the water layer extracted 3 × 10 ml of EA. The combined organic layers were dried by standing over Na_2SO_4, filtered and evaporated to dryness by RVE and HV. An obtained solid material was separated by FLC (SiO_2, EA:Hex (2:1)). The product 26.0 mg (0.051 mmol, 52.0%) **8** was a white powder. Mp: 183.0–186.0 °C [EA]. IR ν (solid, cm^{-1}): 3342 (w, NH), 3102 (m), 2923 (m), 1602 (m), 1575 (s), 1425 (m), 1306 (m, S=O), 1263 (m), 1122 (s, S=O), 1083 (m), 1020 (w), 734 (m), 717 (m). ^{1}H NMR (300 MHz, DMSO-d_6): δ 9.92 (s, 1H, NH), 8.80 (d, 1H, J(4,6) = 2.3 Hz, H–C(6)), 8.72 (ddd, 1H, J(5″,6″) = 4.8 Hz, J(4″,6″) = 1.8 Hz, J(3″,6″) = 0.9 Hz, H–C(6″)), 8.36 (dd, 1H, J(2′,4′) = J(2′,6′) = 1.5 Hz, H–C(6′)), 8.15 (dd, 1H, J(2′,4′) = J(4′,6′) = 1.5 Hz, H–C(4′)), 8.11 (ddd, 1H, J(3″,4″) = 8.0 Hz, J(3″,5″) = J(3″,6″) = 0.9 Hz, H–C(3″)), 7.96 (ddd, 1H, J(3″,4″) = 8.0 Hz, J(4″,5″) = 7.8 Hz, J(4″,6″) = 1.8 Hz, H–C(4″)), 7.92 (dd, 1H, J(2′,4′) = J(2′,6′) = 1.5 Hz, H–C(2′)), 7.80 (s, 1H, H–C(4_{ox})), 7.52 (dd, 1H, J(3,4) = 8.6 Hz, J(4,6) = 2.3 Hz, H–C(4)), 7.45 (ddd, 1H, J(4″,5″) = 7.8 Hz, J(5″,6″) = 4.8 Hz, J(3″,5″) = 0.9 Hz, H–C(5″)), 7.29 (d, 1H, J(3,4) = 8.6 Hz, H–C(3)), 4.00 (s, 3H, –OCH_3), 3.22 (q, 2H, J (CH_2,CH_3) = 7.2 Hz, –CH_2–), 1.13 (t, 3H, J (CH_2,CH_3) = 7.2 Hz, –CH_3). ^{13}C NMR (75 MHz, DMSO-d_6): δ 155.5 (C2″), 155.2 ($C2_{ox}$), 150.5 (C2), 149.6 (C6″), 144.0 ($C5_{ox}$), 141.8 (C5′), 137.1 (C4″), 132.4 (C5), 131.0 (C1), 130.9 (C2′), 128.6 (C4′), 126.0 (C6′), 123.5 (C3′), 123.0 (C5″), 122.7 ($C4_{ox}$), 120.8 (C3″), 120.0 (C4), 115.4 (C6), 109.6 (C3), 56.3 (–OCH_3), 50.7 (–CH_2–), 7.6 (–CH_3). Anal. calcd. for $C_{23}H_{20}BrN_3O_4S$ (514.39): C, 53.70; H, 3.92; Br, 15.53; N, 8.17; S, 6.23; found: C, 53.52; H, 3.86; Br, 15.57; N, 8.00; S, 6.02.

4.2.12. N-[5-(Ethylsulfonyl)-2-methoxyphenyl]-5-[3-(pyridin-2-yl)-5-(pyridin-3-yl)phenyl]oxazol-2-amine (**23ASYM**)

The mixture of 50.0 mg (0.097 mmol, 1.00 mol eq) 5-(3-bromo-5-(pyridin-2-yl)phenyl)-*N*-(5-(ethylsulfonyl)-2-methoxyphenyl) oxazol-2-amine (**8**), 31.0 mg (0.097 mmol, 1.00 mol eq) tetrabutylammonium bromide, 7.0 mg (0.0061 mmol, 0.062 mol eq) tetrakis(triphenylphosphine)palladium(0), 36.0 mg (0.097 mmol, 1.00 mol eq) 3-(tributylstannyl)pyridine in 1 ml of AN was sealed under Ar and heated by stirring at 100 °C for 48 h. After cooling, the tube was opened and its content washed out with 25 ml of EA. Then 10 ml of 1 M aqueous KF solution was added to EA suspension and stirred for 3 h at rt. The organic layer was separated and the water layer extracted with 3 × 10 ml of EA. The combined organic layer was dried by standing over an anhydrous Na_2SO_4, filtered and evaporated by RVE and later on by HV to dryness. The crude mixture was separated by FLC (SiO_2; EA:Hex (2:1)). The required product 31.0 mg (0.060 mmol, 62.3%) **23ASYM** was obtained in a form of a white powder. Mp: 195.0–197.0 °C [FLC]. IR ν (solid, cm^{-1}): 3398 (w, NH), 2939 (w), 1610 (s), 1575 (s), 1526 (m), 1488 (w), 1429 (m), 1301 (m, S=O), 1265 (s), 1142 (s), 1123 (s), 1083 (m), 1020 (w). ^{1}H NMR (300 MHz, DMSO-d_6): δ 8.98 (d, 1H, J(2‴,4‴) = 1.7 Hz, H–C(2‴)), 8.89 (d, 1H, J(4,6) = 2.1 Hz, H–C(6)), 8.76 (ddd, 1H, J(5″,6″) = 4.9 Hz, J(4″,6″) = 1.8 Hz, J(3″,6″) = 0.9 Hz, H–C(6″)), 8.67 (dd, 1H, J(5‴,6‴) = 4.9 Hz, J(4‴,6‴) = 1.5 Hz, H–C(6‴)), 8.25 (dd, 1H, J(2′,4′) = 1.7 Hz, J(2′,6′) = 1.5 Hz, H–C(2′)), 8.12 (dd, 1H, J(4′,6′) = 1.7 Hz, J(2′,6′) = 1.5 Hz, H–C(6′)), 8.05 (ddd, 1H, J(4‴,5‴) = 7.7 Hz, J(2‴,4‴) = 1.7 Hz, J(4‴,6‴) = 1.5 Hz, H–C(4‴)), 7.91 (ddd, 1H, J(3″,4″) = 7.9 Hz, J(3″,5″) = 1.4 Hz, J(3″,6″) = 0.9 Hz, H–C(3″)), 7.85 (ddd, 1H, J(3″,4″) = 7.9 Hz, J(4″,5″) = 7.4 Hz, J(4″,6″) = 1.8 Hz, H–C(4″)), 7.82 (dd, 1H, J(2′,4′) = J(4′,6′) = 1.7 Hz, H–C(4′)), 7.72 (s br, 1H, NH), 7.59 (dd, 1H, J(3,4) = 8.7 Hz, J(4,6) = 2.1 Hz, H–C(4)), 7.44 (dd, 1H, J(4‴,5‴) = 7.7 Hz, J(5‴,6‴) = 4.9 Hz, H–C(5‴)), 7.37 (s, 1H, H–C(4_{ox})), 7.32 (ddd, 1H, J(4″,5″) = 7.4 Hz, J(5″,6″) = 4.9 Hz, J(3″,5″) = 1.4 Hz, H–C(5″)), 7.03 (d, 1H, J(3,4) = 8.7 Hz, H–C(3)), 4.05 (s, 3H, –OCH_3), 3.17 (q, 2H, J(CH_2,CH_3) = 7.3 Hz, –CH_2–), 1.30 (t, 2H, J(CH_2,CH_3) = 7.3 Hz, –CH_3). ^{13}C NMR (75 MHz, DMSO-d_6) δ: 156.3 (C2″), 156.1 ($C2_{ox}$), 150.5 (C2), 149.8 (C6″), 148.9 (C2‴), 148.3 (C6‴), 143.7 ($C5_{ox}$), 140.9 (C3′), 139.2 (C5′), 137.1 (C4″), 136.1 (C4‴), 134.8 (C3‴), 131.0 (C1), 129.4 (C5), 128.8 (C1′), 124.8 (C4′), 123.7 (C6′), 122.9 (C2′), 122.8 (C5″), 122.7 ($C4_{ox}$), 121.2 (C5‴), 120.9 (C3″), 120.1 (C4), 115.3 (C6), 109.6 (C3), 56.3 (–OCH_3), 50.7 (–CH_2–), 7.6 (–CH_3). Anal. calcd. for $C_{28}H_{24}N_4O_4S$ (512.58): C, 65.61; H, 4.72; N, 10.93; S, 6.26; found: C, 65.19; H, 4.61; N, 10.88; S, 6.13.

4.3. Biological evaluation

4.3.1. Materials

Bovine aortic endothelial cells (BAEC) were obtained by collagenase digestion and maintained in Dulbecco's modified Eagle's medium (DMEM) containing glucose (1 g/L), glutamine (2 mM), penicillin (50 IU/mL), streptomycin (50 μg/mL) and amphoterycin (1.25 μg/mL) supplemented with 10% FBS. All the cancer cell lines used in this study were obtained from the American Type Culture Collection (ATCC). Human fibrosarcoma HT1080 cells were

maintained in DMEM containing glucose (4.5 g/L), glutamine (2 mM), penicillin (50 IU/mL), streptomycin (50 μg/mL), and amphotericin (1.25 μg/mL) supplemented with 10% FBS. Human colon adenocarcinoma HT29 and human osteosarcoma U2-OS cells were maintained in McCoy's 5A medium containing glutamine (2 mM), penicillin (50 IU/mL), streptomycin (50 μg/mL), and amphotericin (1.25 μg/mL) supplemented with 10% FBS. Human breast cancer carcinoma MDAMB231 and human promyelocytic leukaemia HL60 cells were maintained in RPMI1640 medium containing glutamine (2 mM), penicillin (50 IU/mL), streptomycin (50 μg/mL) and amphotericin (1.25 μg/mL) supplemented with 10 and 20% FBS, respectively. Compound **22SYM** was dissolved in dimethylsufoxide (DMSO) at a concentration of 10 mM and stored at −20 °C until use.

4.3.2. *In vitro VEGFR2 kinase assay*

A radiometric protein kinase assay (^{33}PanQinase® Activity Assay) was used for measuring the kinase activity of the VEGFR2 protein kinase. VEGFR2 tyrosine kinase was expressed in Sf9 insect cells as human recombinant GST-fusion protein. The kinase was purified by affinity chromatography using GSH-agarose. The purity of the kinase was checked by SDS-PAGE/silver staining and the identity of the kinase was verified by mass spectroscopy. The IC_{50} profile for screened compounds was determined by testing 10 concentrations (1×10^{-4} M to 3×10^{-9} M) for each compound. The measurements have been performed by ProQinase Company [13].

4.3.3. *Cell proliferation assay*

The 3-(4,5-dimethylthiazol-2-yl)-2,5-diphenyltetrazolium bromide (MTT; Sigma Chemical Co., St. Louis, MO) dye reduction assay in 96-well microplates was used, as previously described [24]. 3×10^3 BAE or 2×10^3 tumour cells in a total volume of 100 μL of their respective growth media were incubated with serial dilutions of **22SYM**. After 3 days of incubation (37 °C, 5% CO_2 in a humid atmosphere) 10 μl of MTT (5 mg/ml in PBS) were added to each well and the plate was incubated for a further 4 h (37 °C). The resulting formazan was dissolved in 150 μL of 0.04 N HCl 2-propanol and read at 550 nm. All determinations were carried out in triplicate. IC_{50} value was calculated as the concentration of compound yielding a 50% of cell survival.

4.3.4. *Endothelial cell migration assay*

The migratory activity of BAE cells was assessed using a wound migration assay [25]. Confluent monolayers in 6-well plates were wounded with pipette tips giving rise to one acellular 1 mm-wide lane per well. After washing, cells were supplied with 1.5 mL complete medium in the absence (controls) or presence of the indicated concentrations of **22SYM**. Wounded areas were photographed at zero time and after 7 h of incubation, plates were observed under microscope and photos were taken from the same areas as those recorded at zero time.

4.3.5. *Endothelial cell differentiation assay: tube formation on Matrigel*

Matrigel (50 μL of about 10.5 mg/mL) at 4 °C was used to coat each well of a 96-well plate and allowed to polymerize at 37 °C for a minimum of 30 min as described previously [26]. Some 5×10^4 BAE cells were added with 200 μL of DMEM. Finally, different amounts of **22SYM** were added and incubated at 37 °C in a humidified chamber with 5% CO_2. After incubation for 7 h, cultures were observed (200× magnification) and photographed with a NIKON inverted microscope DIAPHOT-TMD (NIKON Corp., Tokyo, Japan). Each concentration was tested in duplicate, and two different observers evaluated the results of tube formation inhibition.

4.3.6. *Hoechst staining*

Cells were plated on 8-well chamber slides and grown to subconfluence. After treatments for 14 h with the indicated concentrations of **22SYM** in complete medium, cells were washed with PBS and fixed with formalin solution. Chamber slides were stained with 1 mg/mL Hoechst in PBS for 2 min, washed twice with PBS and mounted (DAKO Cytomation Fluorescent Mounting Medium, Denmark). Samples were observed under a fluorescence microscope (Leica, TCS-NT, Heidelberg, Germany).

4.3.7. *In vivo Zebrafish embryo assay*

To evaluate the *in vivo* antiangiogenic activity, different concentrations of screened compound were incubated with embryos from a transgenic (TG(fli1:EGFP)y1) Zebrafish line that carries a 15-kb promoter of the transcription factor friend leukaemia virus integration-1 (fli-1), which drives the GFP expression in the endothelium. The systemic exposure of screened compound can exerted a dose–response inhibitory effect on the developmental angiogenesis in Zebrafish. During development of the Zebrafish, intersegmental vessels sprout and grow upward from the aorta, and then the tips join by anastomosis to form a dorsal vein. The embryos should remain viable during the 24-h period of the study and overall morphology should be similar to control embryos, indicating that development was unaffected and also indicating a low toxicity of screened compound. *In vivo* live fluorescent Zebrafish embryo assay was carried out with different doses of screened compound. Data are given as percentage of embryos with inhibited angiogenesis per total number of treated Zebrafish embryos.

Acknowledgements

This work was supported by VEGA grant 1/0634/13. We are grateful for the gift of drug active compounds: sorafenib tosylate (Nexavar®, Bayer HealthCare Pharmaceuticals) and sunitinib L-malate (Sutent®, Pfizer Inc.). For molecular docking, structure predictions and TK conclusions, we thank to Biomagi, Ltd. Slovakia. The COST action CM0602 (AngioKem) and CM1106 (StemChem) for research networking is also acknowledged. We would like to thank the Molinspiration Property Calculation Service www.molinspiration.com for drug-like prediction calculations. This work is dedicated to memory of Magdaléna Bohá-čová and prof. Camille Ganter.

Appendix A. Supplementary data

Supplementary data related to this article can be found at http://dx.doi.org/10.1016/j.ejmech.2013.11.023.

References

[1] P. Carmeliet, VEGF as a key mediator of angiogenesis in cancer, Oncology 69 (2005) 4–10. http://dx.doi.org/10.1159/000088478.
[2] S.D. Finley, A.S. Popel, Predicting the effects of anti-angiogenic agents targeting specific VEGF isoforms, AAPS J. 14 (2012) 500–509. http://dx.doi.org/10.1208/s12248-012-9363-4.
[3] P. Hamerlik, J.D. Lathia, R. Rasmussen, Q. Wu, J. Bartkova, M. Lee, P. Moudry, J. Bartek Jr., W. Fischer, J. Lukas, J.N. Rich, J. Bartek, Autocrine VEGF-VEGFR2-Neuropilin-1 signaling promotes glioma stem-like cell viability and tumor growth, J. Exp. Med. 209 (2012) 507–520. http://dx.doi.org/10.1084/jem.20111424.
[4] P.A. Harris, M. Cheung, R.N. Hunter, M.L. Brown, J.M. Veal, R.T. Nolte, L. Wang, W. Liu, R.M. Crosby, J.H. Johnson, A.H. Epperly, R. Kumar, D.K. Luttrell, J.A. Stafford, Discovery and evaluation of 2-anilino-5-aryloxazoles as a novel class of VEGFR2 kinase inhibitors, J. Med. Chem. 48 (2005) 1610–1619. http://dx.doi.org/10.1021/jm049538w.
[5] http://www.rcsb.org/pdb/home/home.do (visited 21st May 2013).

[6] F. Zuccotto, E. Ardini, E. Casale, M. Angiolini, Through the "gatekeeper door": exploiting the active kinase conformation, J. Med. Chem. 53 (2010) 2681–2694. http://dx.doi.org/10.1021/jm901443h.
[7] M.A. McTigue, J.A. Wickersham, C. Pinko, R.E. Showalter, C.V. Parast, A. Tempczyk-Russell, M.R. Gehring, B. Mroczkowski, C.-C. Kan, J.E. Villafranca, K. Appelt, Crystal structure of the kinase domain of human vascular endothelial growth factor receptor 2: a key enzyme in angiogenesis, Structure 7 (1999) 319–330. http://dx.doi.org/10.1016/S0969-2126(99).80042-2.
[8] Molinspiration Property Calculation Service http://www.molinspiration.com/cgi-bin/properties (visited 21st May 2013).
[9] C. Beier, M. Zacharias, Tackling the challenges posed by target flexibility in drug design, Expert Opin. Drug Discovery 5 (2010) 347–359. http://dx.doi.org/10.1517/17460441003713462.
[10] O. Rabal, G. Schneider, J.I. Borrell, J. Teixido, Structure-based virtual screening of FGFR inhibitors: cross-decoys and induced-fit effect, BioDrugs 21 (2007) 31–45.
[11] C.N. Cavasotto, R.A. Abagyan, Protein flexibility in ligand docking and virtual screening to protein kinases, J. Mol. Biol. 337 (2004) 209–225. http://dx.doi.org/10.1016/j.jmb.2004.01.003.
[12] M. Murár, G. Addová, A. Boháč, Synthesis of 5-(ethylsulfonyl)-2-methoxyaniline: an important pharmacological fragment of VEGFR2 and other inhibitors, Beilstein J. Org. Chem. 9 (2013) 173–179. http://dx.doi.org/10.3762/bjoc.9.20.
[13] Determination of enzymatic IC_{50} activity on VEGFR2 receptor has been performed by ProQinase GmbH, Freiburg, Germany http://www.proqinase.com/ (visited 21st May 2013).
[14] L. Garuti, M. Roberti, G. Bottegoni, Non-ATP competitive protein kinase inhibitors, Curr. Med. Chem. 17 (2010) 2804–2821.
[15] http://www.uniprot.org/uniprot/P35968 (visited 15th May 2013).
[16] http://www.rcsb.org/pdb/workbench/workbench.do (visited 15th May 2013)
[17] L.N. Johnson, M.E.M. Noble, D.J. Owen, Active and inactive protein kinases: structural basis for regulation, Cell 85 (1996) 149–158. http://dx.doi.org/10.1016/S0092-8674(00).81092-2.
[18] J.J. Irwin, B.K. Shoichet, M.M. Mysinger, N. Huang, F. Colizzi, P. Wassam, Y. Cao, Automated docking screens: a feasibility study, J. Med. Chem 52 (2009) 5712–5720. http://dx.doi.org/10.1021/jm9006966.
[19] http://dock.compbio.ucsf.edu/DOCK3.6/(visited 21st May 2013).
[20] Y. Miura, M. Momoki, M. Nakatsuji, Y. Teki, Stable thioaminyl radicals having functional groups: generation, ESR spectra, isolation, X-ray crystallographic analyses, and magnetic characterization of *N*-(arylthio)-4-(ethoxycarbonyl)-2,6-diarylphenylaminyls, *N*-(arylthio)-4-acetyl-2,6-diarylphenylaminyls, and *N*-(arylthio)-4-cyano-2,6-diarylphenylaminyls, J. Org. Chem 63 (1998) 1555–1565. http://dx.doi.org/10.1021/jo9718206.
[21] M.S. Nery, M.S. Azevedo, J.N. Cardoso, G.B.C. Slana, R.S.C. Lopes, C.C. Lopes, A new chemoselective synthesis of brombuterol, Synthesis 39 (2007) 1471–1474. http://dx.doi.org/10.1055/s-2007-966044.
[22] T.M. Miller, T.X. Neenan, R. Zayas, H.E. Bair, Synthesis and characterization of a series of monodisperse, 1,3,5-phenylene-based hydrocarbon dendrimers including C276H186 and their fluorinated analogs, J. Am. Chem. Soc. 114 (1992) 1018–1025. http://dx.doi.org/10.1021/ja00029a034.
[23] R.E. Lutz, R.K. Allison, G. Ashburn, P.S. Bailey, M.T. Clark, J.F. Codington, A.J. Deinet, J.A. Freek, R.H. Jordan, N.H. Leake, T.A. Martin, K.C. Nicodemus, R.J. Rowlett Jr., N.H. Shearer Jr., J.D. Smith, J.W. Wilson III, J. Org. Chem. 12 (1947) 617–680.
[24] S. Rodriguez-Nieto, M.A. Medina, A.R. Quesada, A re-evaluation of fumagillin selectivity towards endothelial cells, Anticancer Res. 21 (2001) 3457–3460.
[25] B. Martinez-Poveda, A.R. Quesada, M.A. Medina, Hypericin in the dark inhibits key steps of angiogenesis in vitro, Eur. J. Pharmacol. 516 (2005) 97–103. http://dx.doi.org/10.1016/j.ejphar.2005.03.047.
[26] S. Rodriguez-Nieto, M. Gonzalez-Iriarte, R. Carmona, R. Munoz-Chapuli, M.A. Medina, A.R. Quesada, Anti-angiogenic activity of aeroplysinin-1, a brominated compound isolated from a marine sponge, FASEB J. 16 (2002) 261–263. http://dx.doi.org/10.1096/fj.01-0427fje.